Intermediate Temperature Solid Oxide Fuel Cell Development

Final Report

Contract No. DE-FG26-05NT42471

Period of Performance: July 15, 2005 – June 30, 2008

October 2008

Principal Investigator

S. Elangovan

Phase II Subcontractors

Northwestern University (Prof. Scott Barnett)

California Institute of Technology (Prof. Sossina Haile)

Ceramatec, Inc.

2425 South 900 West

Salt Lake City, UT 84119-1517

Abstract

Solid oxide fuel cells (SOFCs) are high efficiency energy conversion devices. Present materials set, using yttria stabilized zirconia (YSZ) electrolyte, limit the cell operating temperatures to 800°C or higher. It has become increasingly evident however that lowering the operating temperature would provide a more expeditious route to commercialization. The advantages of intermediate temperature (600 to 800°C) operation are related to both economic and materials issues. Lower operating temperature allows the use of low cost materials for the balance of plant and limits degradation arising from materials interactions. When the SOFC operating temperature is in the range of 600 to 700°C, it is also possible to partially reform hydrocarbon fuels within the stack providing additional system cost savings by reducing the air preheat heat-exchanger and blower size.

The promise of Sr and Mg doped lanthanum gallate (LSGM) electrolyte materials, based on their high ionic conductivity and oxygen transference number at the intermediate temperature is well recognized. The focus of the present project was two-fold: a) Identify a cell fabrication technique to achieve the benefits of lanthanum gallate material, and b) Investigate alternative cathode materials that demonstrate low cathode polarization losses at the intermediate temperature. A porous matrix supported, thin film cell configuration was fabricated. The electrode material precursor was infiltrated into the porous matrix and the counter electrode was screen printed. Both anode and cathode infiltration produced high performance cells. Comparison of the two approaches showed that an infiltrated cathode cells may have advantages in high fuel utilization operations.

Two new cathode materials were evaluated. Northwestern University investigated LSGM – ceria composite cathode while Caltech evaluated Ba-Sr-Co-Fe (BSCF) based pervoskite cathode. Both cathode materials showed lower polarization losses at temperatures as low as 600°C than conventional manganite or cobaltite cathodes.

SBIR RIGHTS NOTICE

These SBIR data are furnished with SBIR rights under Grant No. DE-FG26-05NT42471. For a period of 4 years after acceptance of all items to be delivered under this grant, the Government agrees to use these data for Government purposes only, and they shall not be disclosed outside the Government (including disclosure for procurement purposes) during such period without permission of the grantee, except that, subject to the foregoing use and disclosure prohibitions, such data may be disclosed for use by support contractors. After the aforesaid 4-year period the Government has a royalty-free license to use, and to authorize others to use on its behalf, these data for Government purposes, but is relieved of all disclosure prohibitions and assumed no liability for unauthorized use of these data by third parties. This Notice shall be affixed to any reproductions of these data in whole or in part.

(End of Notice)

Table of Contents

CHAPTER 1. INTRODUCTION 1-1
ELECTRODE MATERIALS 1-1
STRENGTH 1-2
CELL DESIGN 1-2
COST 1-3
CELL PERFORMANCE 1-5
CATHODE MATERIAL 1-6

CHAPTER 2. CERAMATEC ACTIVITIES 2-1
FABRICATION OF CELL PACKAGE 2-1
NARROW SPACING FOR SUPPORT LAYER 2-1
ELECTRODE INFILTRATION PROCESS DEVELOPMENT 2-2
GALLATE HALF CELL TESTING 2-4
CELL SIZE SCALE UP 2-6
INTERCONNECT COATING 2-6
STACK TEST 2-8
CONCLUSIONS 2-9

CHAPTER 3. CATHODE DEVELOPMENT AT NORTHWESTERN UNIVERISTY 3-1
INTRODUCTION 3-1
EXPERIMENTAL PROCEDURE 3-1
Fabrication of Electrolyte Support Pellets 3-1
Preparation of Symmetrical Cells 3-1
Electrochemical Characterization 3-1
RESULTS AND DISCUSSION 3-2
Chemical Compatibility of LSGM and LSCF 3-2
Effect of Sintering Temperature 3-3
Effect of Cathode Composition 3-4
Effect of Oxygen Partial Pressure 3-7
Stability of LSCF-LSGM Composite Cathode 3-8
LSCF-LSGM composite cathode performance in an anode-supported SOFC 3-9
EXPERIMENTAL PROCEDURE 3-10
RESULTS AND DISCUSSION 3-11
TESTING OF CALTECH CATHODE MATERIALS 3-15
SUMMARY AND CONCLUSIONS 3-17

CHAPTER 4. CATHODE DEVELOPMENT AT CALTECH 4-1
Introduction 4-1
Sample Preparation and Phase Characterization 4-1
Electrochemical Characterization 4-4
Conclusions 4-9

Chapter 1. Introduction

The benefits of lowering the operating temperature of solid oxide fuel cells (SOFC) are well recognized. Some of those benefits include: improvement in long-term stability by slowing physical and chemical changes in the cell materials, lower cost systems by the use of smaller heat exchangers made from low cost materials, compatibility with hydrocarbon reformation process allowing partial internal reformation which further reduces the heat exchanger duty, and finally the potential to improve thermal cycle capability. In addition, the lower operating temperature also facilitates the use of inexpensive stainless steel interconnects. A temperature range of 650 to 700°C is ideally suited to derive the performance stability, system integration and cost benefits.

In order to derive the advantages of the lower operating temperature, two factors that limit the cell performance, namely the electrolyte resistance and electrode polarization must be addressed. Traditional yttria-doped zirconia (YSZ) electrolyte has been shown to perform at high power density at 800°C in an anode-supported thin film configuration. Further reduction in operating temperature has posed a considerable challenge because of the increased losses at the cathode/electrolyte interface. Lanthanum gallate compositions have shown high oxygen ion conductivity when doped with Sr and Mg. Unlike other oxygen ion conductors such as ceria and bismuth oxide, the Sr and Mg doped lanthanum gallate (LSGM) compositions are stable over the oxygen partial pressure range of interest. The combination of stability in low pO_2 and the high oxygen ion conductivity with a transference number close to unity makes the LSGM material a potential choice for intermediate temperature SOFCs. However, challenges in the development of electrode materials and cell fabrication processes need to be addressed to make use of the potential of the LSGM electrolyte.

Electrode Materials

In Phase I of the project, the nickel anode was modified to make a solid solution of NiO-MgO as the starting material. The approach was used to make use of the common element in the anode and the LSGM electrolyte such that the driving force for Ni-La reaction is lowered. During the cell start-up the NiO component of the anode would reduce leaving nickel grains containing a fine dispersion of MgO particles. The dispersoid has the additional benefit of retarding the coarsening of nickel grains, providing long-term microstructural stability. Powder mixtures of the solid solution, NiO-MgO, and the LSGM showed a significant reduction in the reactivity even at a calcination temperature of 1300^{o}C. In Phase II, the long-term durability of the modified anode was demonstrated by operating several button cells for over 1,000 hours at power densities of 500 mW/cm^2.

During Phase I and Phase II, Sr-doped $LaCoO_3$ (LSCo) was used as the cathode. The selection of LSCo was based on its performance as an excellent intermediate temperature cathode. However, stack tests in Phase II showed the propensity of LSCo to be poisoned by Cr from the interconnect. Two effects were observed: a) reaction of Sr in the current collection LSCo layer to form a Sr-Cr rich oxide layer on the top surface and distribution of Cr-rich phase through the electrode and at the electrode/electrolyte interface. Although, in the SECA CTP program efforts are underway to minimize Cr evaporation from the interconnect, it may be beneficial to modify the cathode to be less susceptible to chromium poisoning. This could be accomplished either through compositional modification of the cathode, graded composition

where the layer in proximity to the metal interconnect is less susceptible to reactivity, or through design modification to limit chromium access to the cathode/electrolyte interface.

Strength

The mechanical strength of the electrolyte material is critical in the reliability of the SOFC stack. This is particularly important as thinner electrolyte is employed to lower the electrolyte ohmic contribution. Previous published results of LSGM strength indicate an average strength of about 140 MPa. It is well understood that the strength of ceramic material is highly dependent on flaw size, which in turn depends on the fabrication technique. Following ASTM standard technique, 4-point strength tests at various conditions were performed at the Sandia National Lab. The strength bar samples were machined from sintered billets. In addition to measuring as-prepared samples, tests were done using samples that were exposed to 800^{o}C in air for 100 hours, in hydrogen for 100 hours, thermal cycled between room temperature and 800^{o}C in air and hydrogen. Finally, as-prepared samples were also tested at 800^{o}C. The results are shown in Figure 1 below. For all conditions, the strength values at room temperature were within the standard deviation of other treatment conditions. The strength value at 800^{o}C was lower, as expected, by about 25%. In general, the room temperature strength values were higher than those reported in the limited available literature data. Almost all test conditions showed the fracture origin to be internal pores or surface flaws. Thus, improvements in powder processing (reduction in agglomerate size), and fabrication (better powder packing) are expected to provide components with fewer and smaller flaws, resulting in much higher strength values. In comparison, the average room temperature strength of 8YSZ is reported to be in the range 200 - 300 MPa.

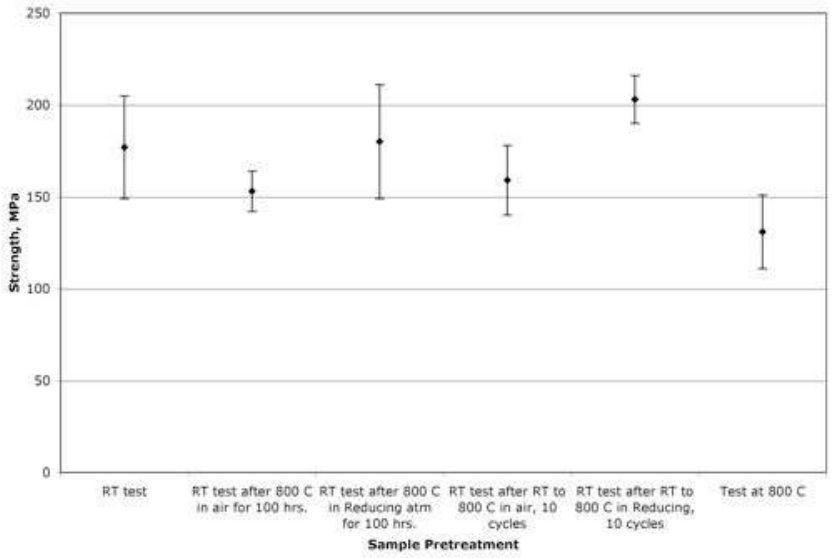

Figure 1. Measured strength of LSGM

Cell Design

The thin electrolyte approach to achieve high performance requires that the electrolyte be supported on a thick electrode. In the case of zirconia-based cells, the anode is used as the support since the anode/YSZ the bilayer can be cosintered. Initial trails using the anode-LSGM

electrolyte bilayer approach indicated even with the modified anode, the sintering temperature was too high to prevent the interfacial reactivity. A subsequent approach employed a cosintered bilayer of a thin electrolyte and porous network of electrolyte as the support. The porous skeleton was infiltrated with an anode precursor and the button cell showed a power density of >500 mW/cm^2 at 700°C. However, the performance was reduced considerably at higher fuel utilizations. A similar performance penalty has also been reported for anode-supported zirconia cells. The cell design was subsequently modified to a multilayer laminate, which when sintered consisted of a thin dense layer supported on a continuous porous layer and by one or more porous slotted layers backed by a slotted dense layer. The porous layer was infiltrated by either anode slurry or cathode slurry to fabricate anode and cathode-supported cells. Anode supported cells showed some warpage upon reduction of NiO. Much of the work then focused on cathode-supported cell design, as they experience no phase change to the electrode during operation. In addition, the compatibility of the cathode and gallate perovskite structure is considered beneficial in that a small amount of Co diffusion into the electrolyte does not change the electrolyte property. The infiltration technique also accommodates the large thermal expansion mismatch between LSGM and LSCo. Micrographs of a cathode-supported cell are shown in Figure 2.

Cost

Raw Material: Using prevailing prices for high purity components of the LSGM electrolyte as reported in the US Geological Survey Minerals Year Book, a preliminary cost model was completed. The electrolyte raw material cost is plotted as a function of power density in a parametric form for various electrolyte thicknesses. For example, at an operating power density of 500 mW/cm^2 an electrolyte thickness of up to 50 microns will result in a raw material cost of under $8/kW while at 100 microns it will cost around $12/kW (Figure 3). Additional cost for the synthesis of the LSGM phase by calcination method is expected to add only a small fraction of the raw material cost.

Fabrication: The process of fabrication involves tape casting, laser featuring of green layers, lamination and sintering of the laminate. The tape casting and lamination processes are well established low cost manufacturing method widely practiced in the electronics industry. At the manufacturing level there are two options for green tape featuring: carbide die punching and laser cutting. The cost of a CNC punch is estimated to be around $200,000 while the die cost is around $25k to $50k depending on whether it is a circular punch or a slot. The circular punch needs to make numerous ‘nibbles’ to achieve the slot pattern. Typical dies last for about 200,000 punches after which they need to be replaced. A continuous tape reel fed laser cutter is estimated to be around $500k and does not require ‘die’ replacements. Assuming the maintenance cost of a CNC punch is comparable to a laser machine, the cost of die replacement is expected to dominate the large volume manufacturing cost. Ceramatec’s industrial partner in a parallel electrochemical system project conducted the cost analysis and chose the fabrication process development based on laser cutting. The continuous reel feed option significantly lowers the labor cost of changing the blanks after each cutting operation. Laser cutting also provides the flexibility of different features for various layers without the need to change the hard tooling or requiring multiple machines.

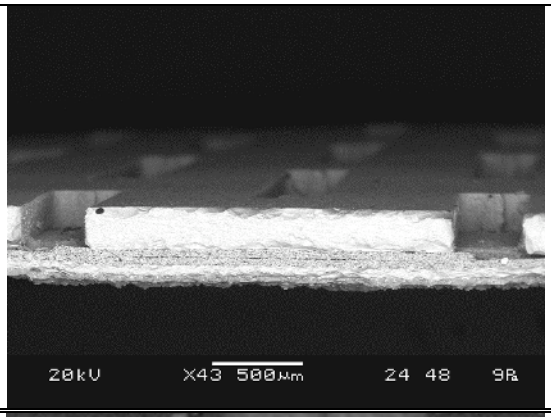	Fractured cross section •Layers (top to bottom in figure) 1. Slotted Dense (200 µm) 2. Slotted Porous (50 µm) 3. Slotted Porous (50 µm) 4. Dense (75 µm)
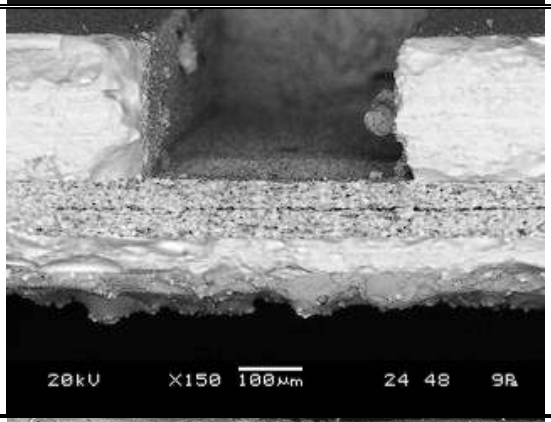	Slot in porous layer visible under dense layer slots
	Screen printed current collection layer to fill the slots
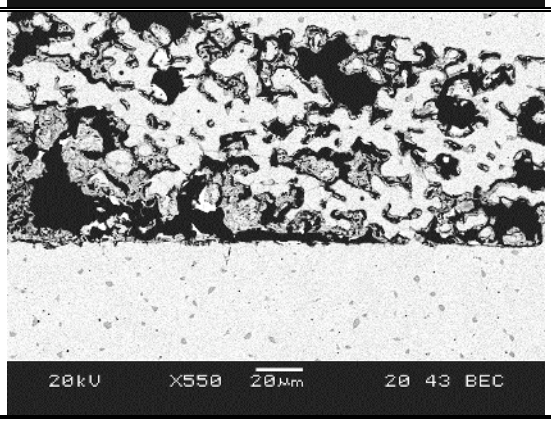	Polished cross section showing composite cathode structure resulting from infiltration of cathode slurry into porous layer. Slotted dense layer is seen on top

Figure 2. Micrographs of cathode-supported LSGM cell

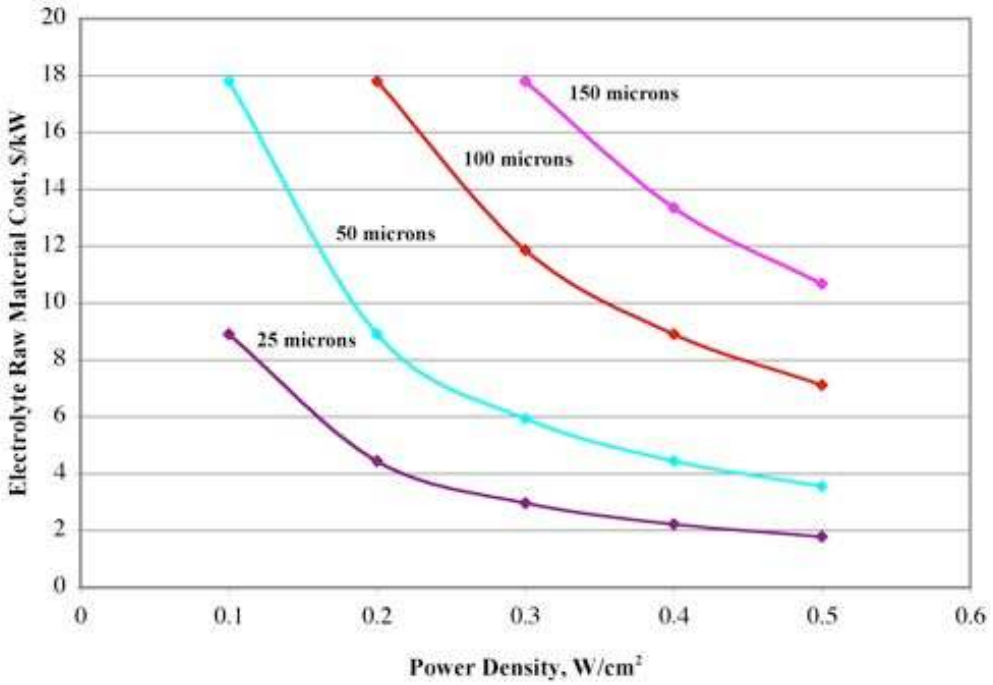

Figure 3. LSGM electrolyte raw material cost estimate

Cell Performance

Button cells were tested using the cathode supported cell design described above. The performance and long-term stability are shown in Figures 4 and 5.

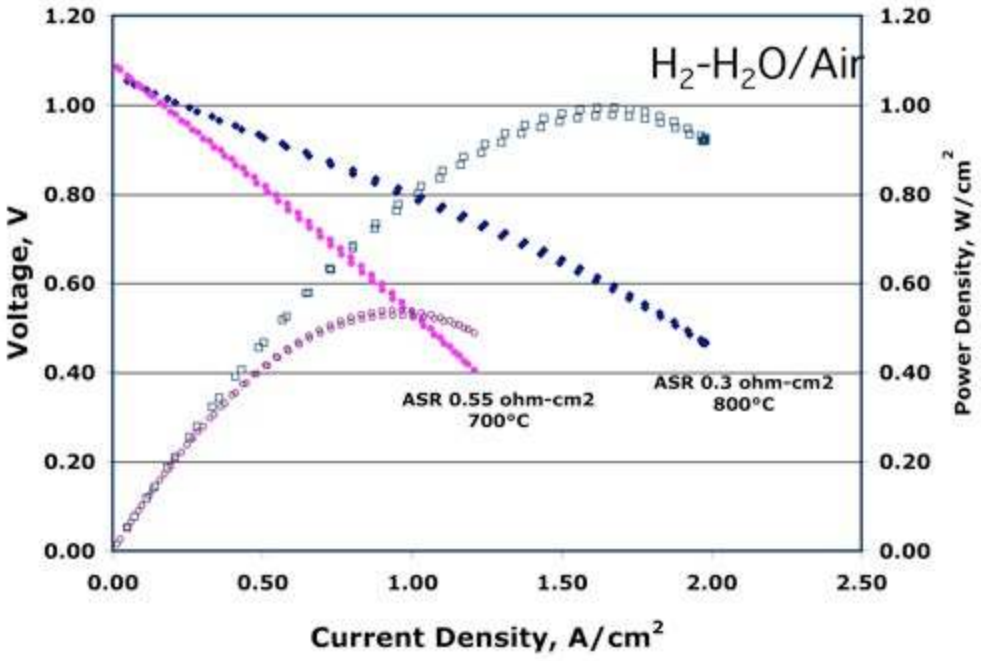

Figure 4. Performance of a cathode-supported LSGM cell

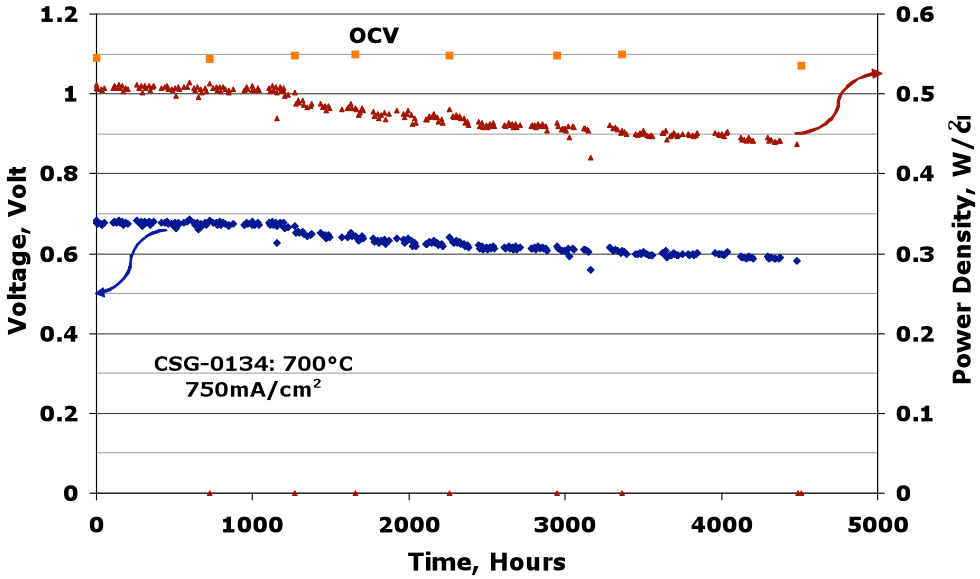

Figure 5. Long-term stability of cathode-supported LSGM cells at 700°C

Cathode Material

While lanthanum cobaltite cathode has good intermediate temperature catalytic activity, the primary issues related to the use of cobaltite cathode are: excessive diffusion of Co into LSGM causing phase destabilization of the electrolyte, and the high CTE of cobaltite compositions. Two alternative cathode compositions have been shown to provide good intermediate temperature performance using ceria electrolyte compositions. They are: $BaSrCoFeO_{3-x}$ at Caltech and $LaSrCoFeO_{3-x}$ at the Northwestern University. These compositions will be evaluated for their cathode performance at the respective Universities under subcontract activities.

Chapter 2. Ceramatec Activities

Fabrication of cell package

The primary approach in making thin electrolyte LSGM cell is by tape casting and laminating a thin dense layer on thick porous layer both made of LSGM. The porous layer can be infiltrated with the appropriate electrode precursor and the opposite electrode can be screen printed. During firing, the precursor forms the desired electrode composition. In general, prior experience with LSGM cells showed that infiltrating cathode is a preferred option since the screen printed anode can be maintained at a lower thickness to improve the gas diffusion properties allowing for high fuel utilization.

High surface area LSGM powder was cast at a green thickness of ~ 25 microns and laminated to a 300 micron green support layer. The packages were then sintered at 1450 C for 6 hours. The 10 micron electrolyte cracked and shrank away in the areas where it was free standing (Figure 6).

Support/cathode side Electrolyte/anode side

Figure 6. Laminate with wider lattice spacing

Sintered dimensions: cell diameter: 3.45 cm
Lattice (solid) width: 0.30 cm
Active area diameter: 2.29 cm

Narrow spacing for support layer

For the second trial with the 25 micron electrolyte layer included a narrower spacing in the slotted pattern for the 300 micron support layer in an attempt to give the electrolyte layer more direct support during the sintering process. A sintered disk is shown in Figure 7.

The cracking/shrinkage issue was improved with the increased support strength, but small cracks are still present in the unsupported areas in the electrolyte layer.

Support/cathode side Electrolyte/anode side

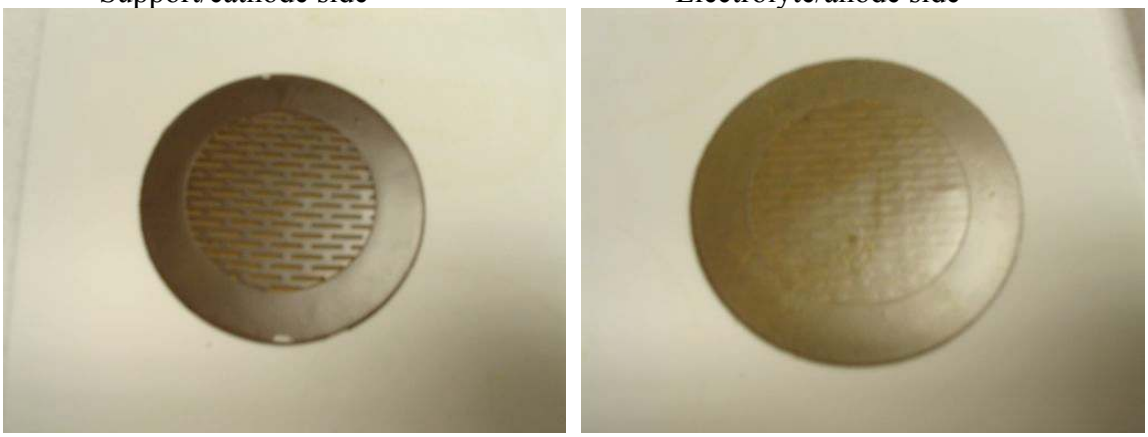

Figure 7. Laminate with narrow lattice spacing

Cell diameter: 3.33 cm
Lattice opening: 0.30 cm (length) x 0.06 cm (width)
Porous opening diameter: 2.18 cm

Electrode infiltration process development.

Using nitrate mixture of cathode cations precursor as an infiltrant was evaluated. The microstructure of a cell with support on the cathode side is shown in Figure 8. Initial trials showed that there are two issues that need to be addressed: 1) the porous support requires additional porosity and 2) the infiltrant does not fully penetrate underneath the lattice.

A surfactant was used to improve the coating characteristics of the infiltrant and the micrographs in Figure 9 show the improved cathode microstructure. A button cell with the new fabrication processes was tested. The cell had an active area of 1 cm^2. The performance curves at different temperatures are shown in Figure 10.

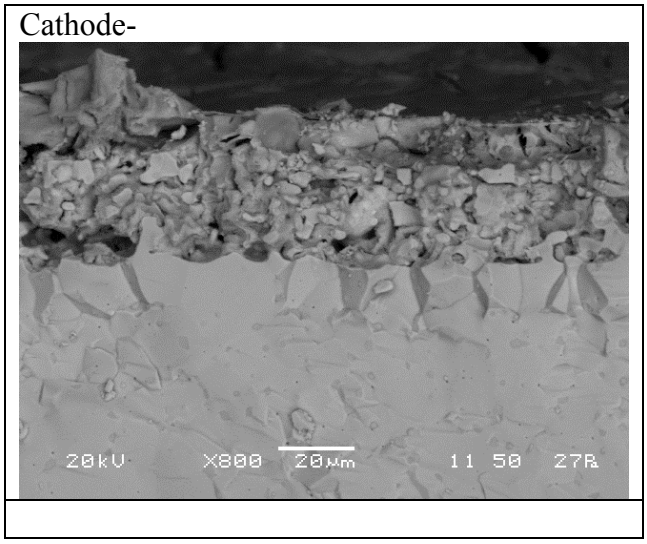

Figure 8. Cathode Structure

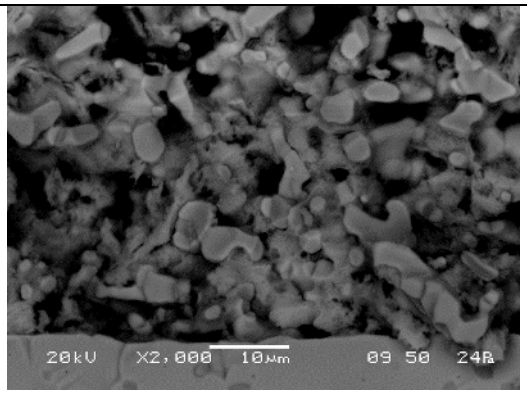

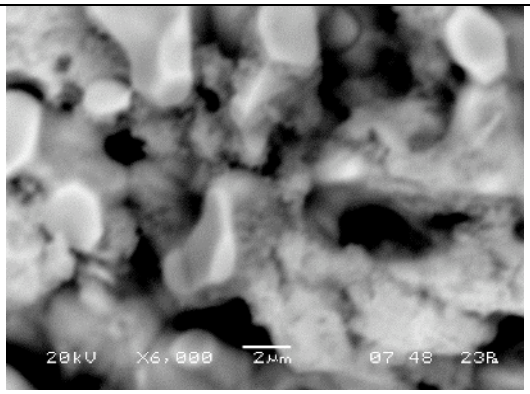

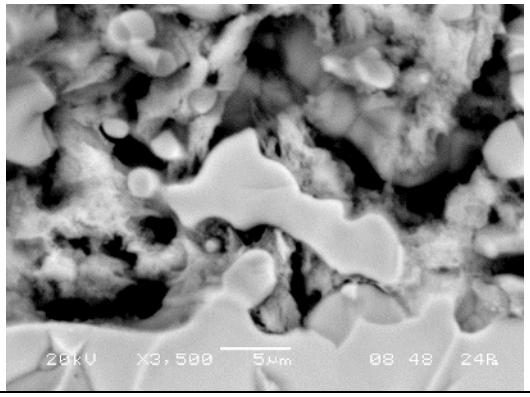

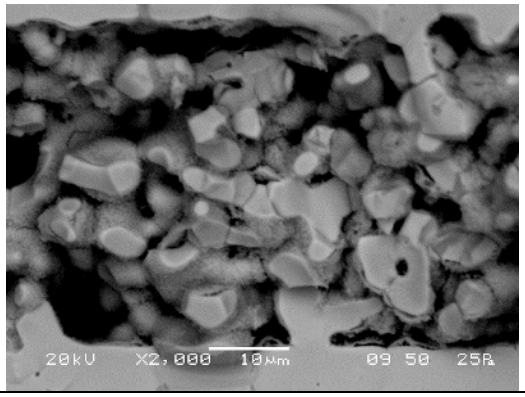

Infiltrated cathode under a slot	Infiltrated cathode under a solid rib

Figure 9. Fracture SEM of improved cathode structure.

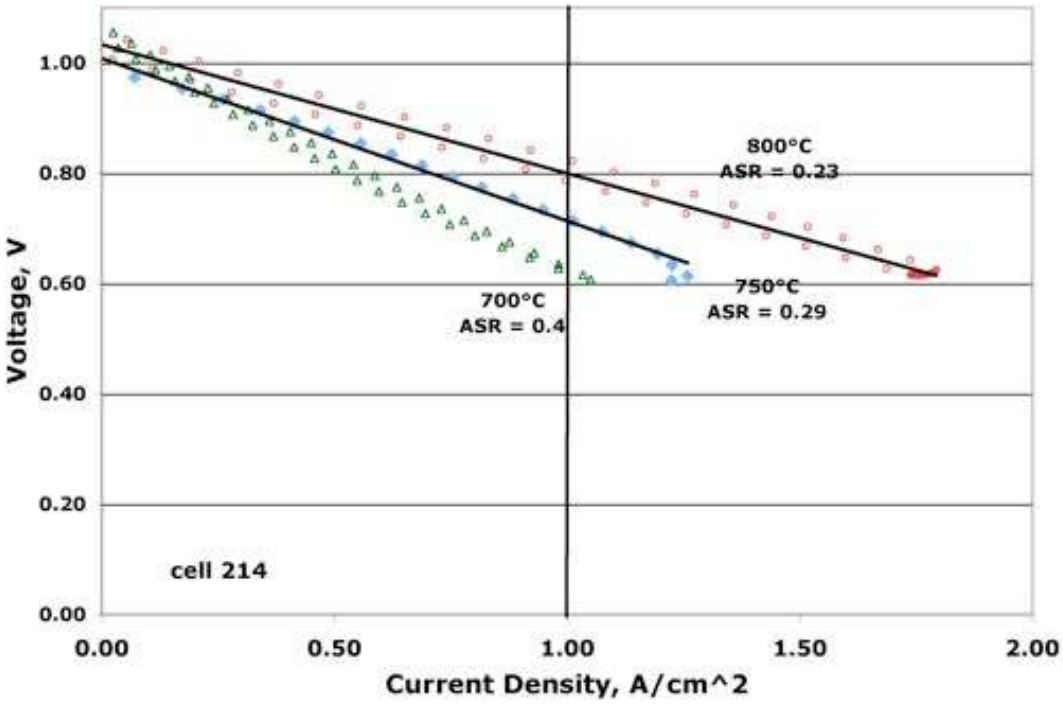

Figure 10. Performance of a button cell with surfactant based cathode infiltration

Gallate Half Cell Testing

Electrolyte supported cathode half cells were fabricated. In addition to testing LSCo ($La_{0.9}Sr_{0.1}CoO_3$) cathode cells, two different modifications (with and without additional $Ce(Gd)O_2$ infiltration or Co nitrate) were also tested. Infiltrated modifications showed a decrease in half cell ASR, as listed in the Table 1 below. Figure 11 shows impedance spectra at 700°C and Figure 12 shows the contributions from the electrolyte and cathode at various temperatures.

Table 1: Gallate - LSCo (La:Sr = 90:10) Half Cells ASR

Process	800°C	750°C	700°C	650°C
No infiltration	.246	.28	.483	1.04
Single Co nitrate	.168	.238	.37	.69
Single GDC	.149	.226	.377	.797
Double Co nitrate	.203	.26	.371	.584
Double GDC	.151	.221	.357	.612

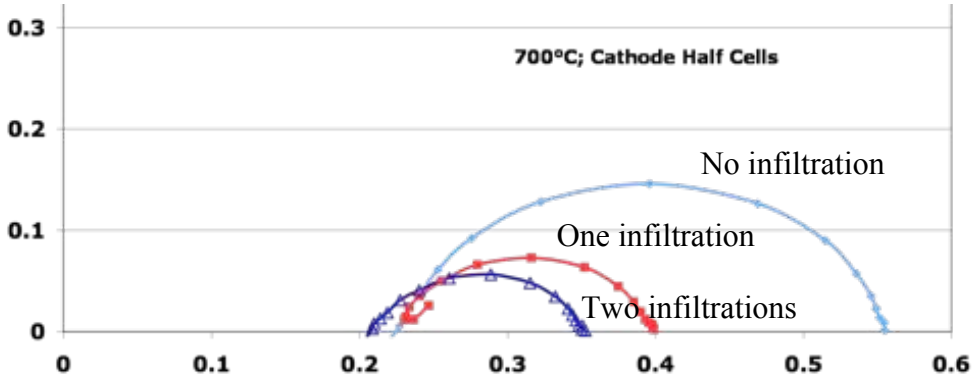

Figure 11. Impedance of cathode half-cells with infiltrations of catalyst (GDC)

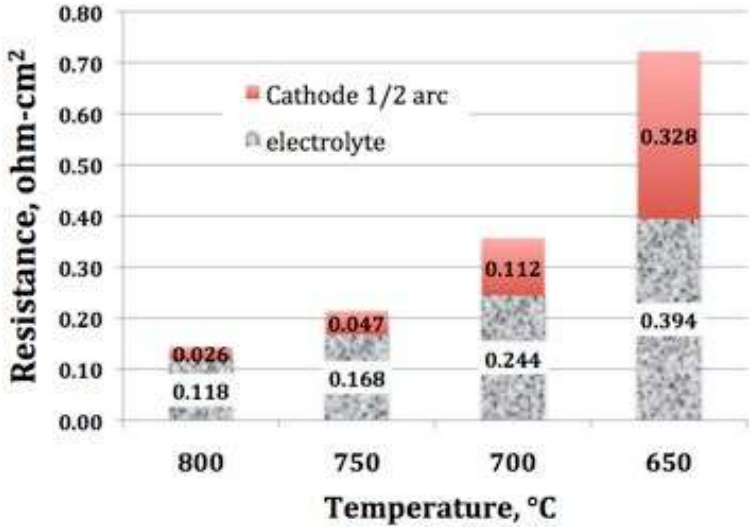

Figure 12. ASR contributions for electrolyte and cathode

Anode optimization

LSGM button cell electrolytes were sintered along with the cathode supported cells. The green electrolyte thickness was 280 microns (11 mils) and the sintered electrolytes were ~ 220 microns.

Two nickel-ceria anode compositions were used to make anode half cells. The anode half cells were tested in humidified (3%) hydrogen inside a quartz tube. Platinum mesh current collectors were used. Among the different combinations, anode composition designated 9010CG (Ni:Mg ratio 9:1) showed the lowest half cell ASR and the results are plotted in Figures 13 and 14.

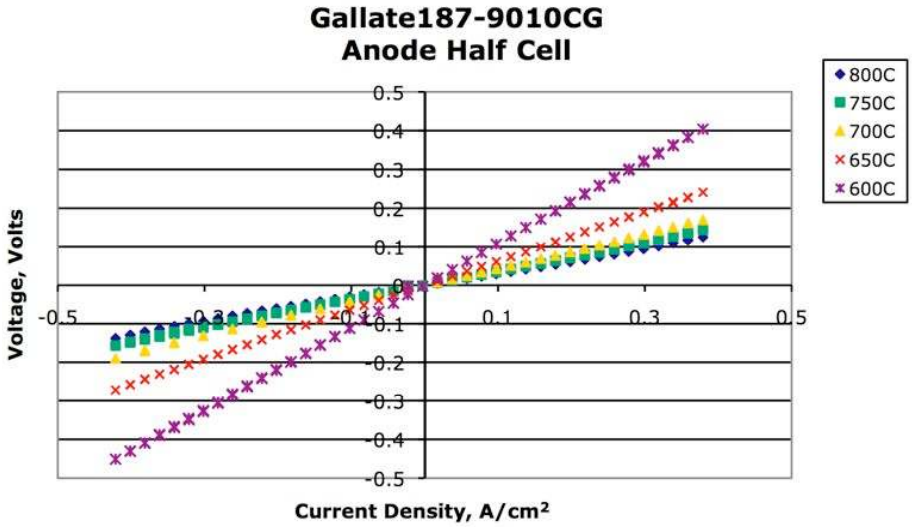

Figure 13. Anode half-cell performance

Temp, °C	DC Polarization ASR
800	.31
750	.37
700	.44
650	.64
600	1.08

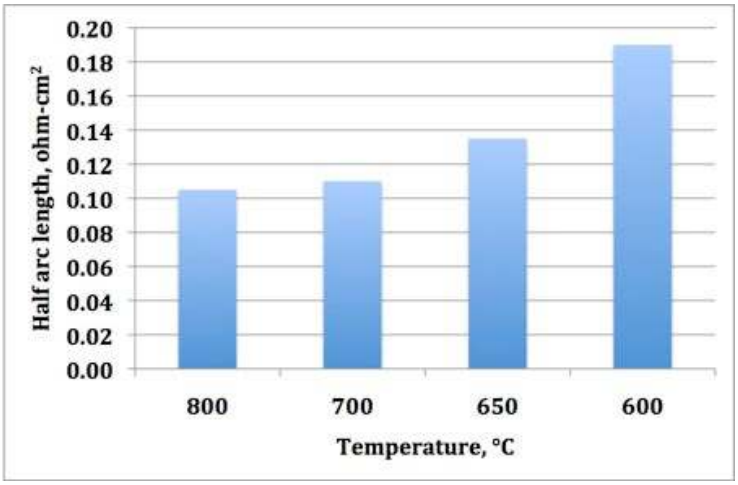

Figure 14. Area specific resistance (Half Arc Length) of anode half cells measured in humidified (3%) hydrogen measured at open circuit condition

Cell Size Scale up

Initial cathode supported cells were tested using a small active area cells and large holes in the support layer over the porous layer. When the active area was increased the cell ASR was found to increase. It is suspected that the in-plane resistance in the infiltrated cathode may be a source for increased ASR, a new group of cathode supported cells have been made to determine the effect of in-plane resistance in the infiltrated porous layer. There are 5 groups of cells with varying diameters – 0.33, 0.64, 1.09, 1.40, and 1.91 cm (0.13, 0.25, 0.43, 0.55, 0.75 inches). The cells were sintered and a one cm square anode was printed and fired. The results of four tested cells are shown in Figure 15. As the diameter increases, the cell ASR decreases, indicating that the cell design must take into account the effect of in-plane resistance. Thus, the full size cell will have to be designed to have the maximum area of direct current collection and still have sufficient strength.

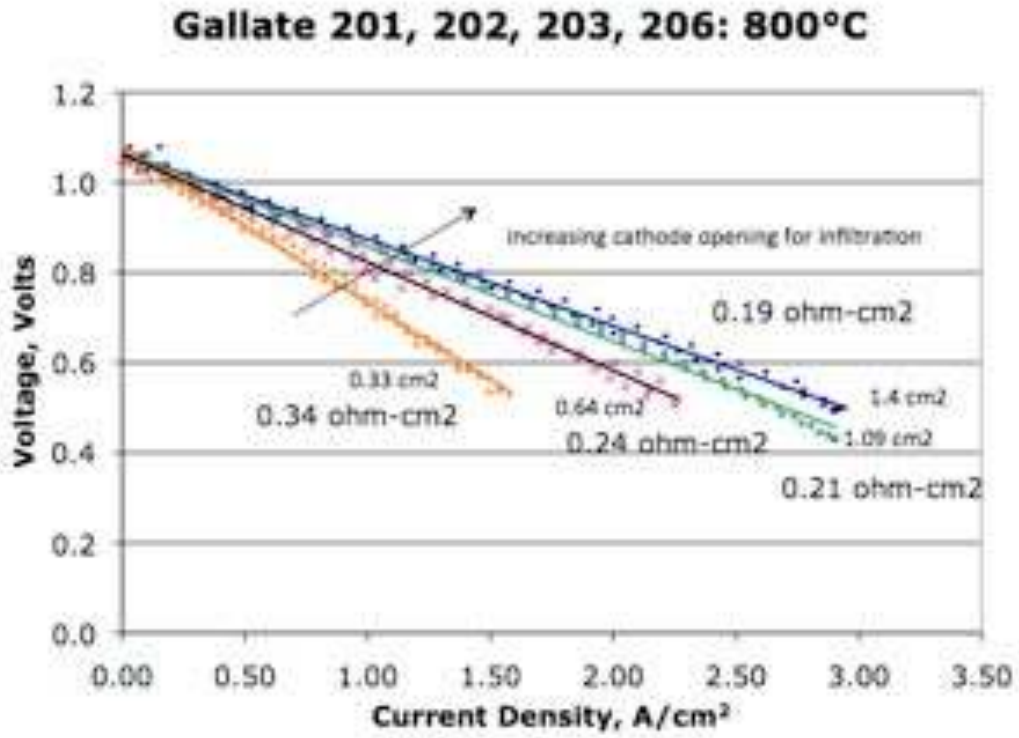

Figure 15. Performance of button cells with varying area in the cathode-side support layer with constant anode area (As the area increases the cell ASR decreases)

Interconnect Coating

Several coupons of stainless plates, with rare earth surface treatment using La nitrate, were sent to PNNL. The samples with Mn-Co spinel coating were received. The coating was analyzed using XRD and SEM/EDS (Figure 16) to confirm the presence of single phase spinel. In addition, two types of configurations were used for conductivity measurements to determine the interfacial resistance of the coated interconnects. In one, a brush painted layer of $La_{0.9}Sr_{0.1}CoO_3$ (LSCo) was fired on top of the spinel at 900°C and a pair of such coupons were couples face to face with a wet LSCo layer. The measurement set up is shown in Figure 17 below.

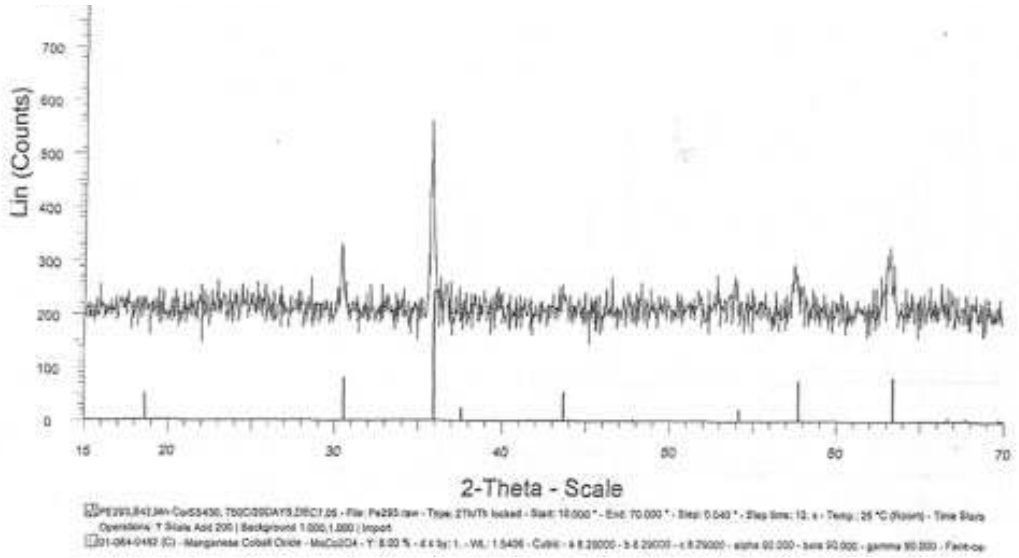

XRD of PNNL Mn-Co spinel coating on stainless steel coupon

EDS-

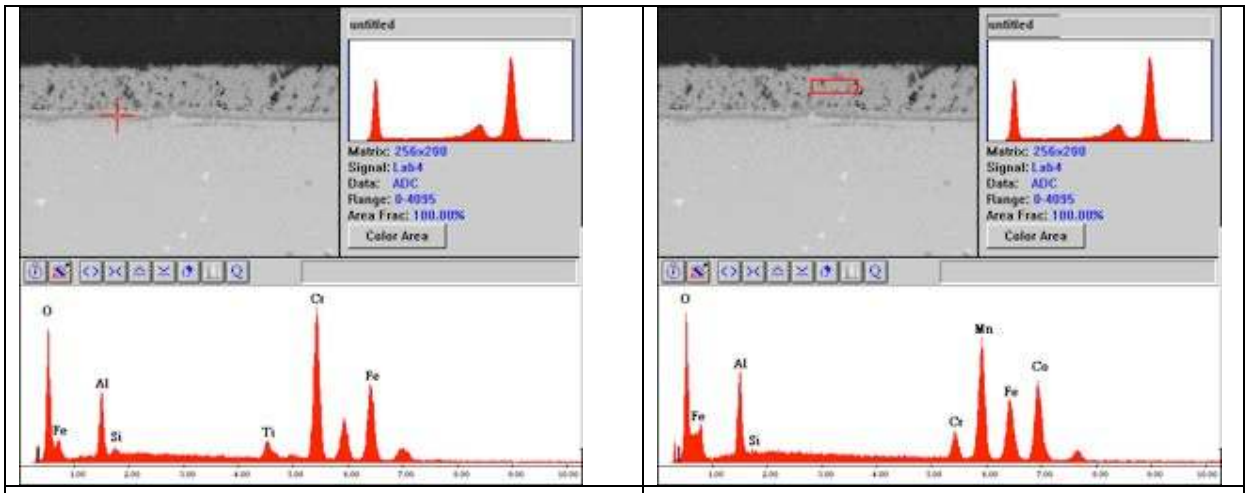

EDS of controlled growth chromium oxide	EDS of MnCo spinel coating from PNNL

XRD and EDS confirm the spinel composition

Figure 16. Characterization of PNNL Spinel Layer

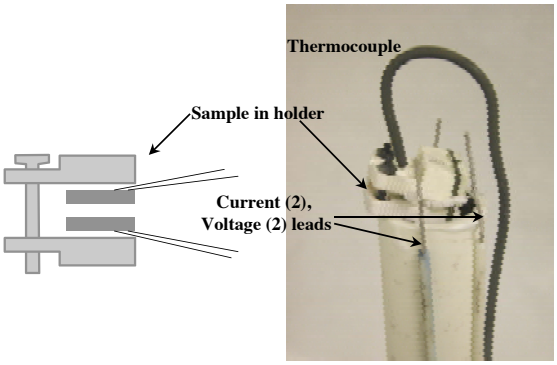

Figure 17. Interface resistance measurement rig

One limitation of the procedure received from PNNL to obtain the spinel coating was the lack of controlled atmosphere furnace suitable for treating 10 x 10 cm components. Modifying the firing atmosphere by firing in nitrogen atmosphere at 900°C for one hour followed by air atmosphere for another hour did not result in an adherent coating.

Instead of Co-Mn spinel, coupons were electrophoretically coated with Cu-Mn spinel. The resistance of coupon couples is shown in Figure 18 for different firing conditions for the coatin, i.e. combinations of nitrogen and air firing for different lengths of time. With the set up shown above, the resistance represents two coated interfaces.

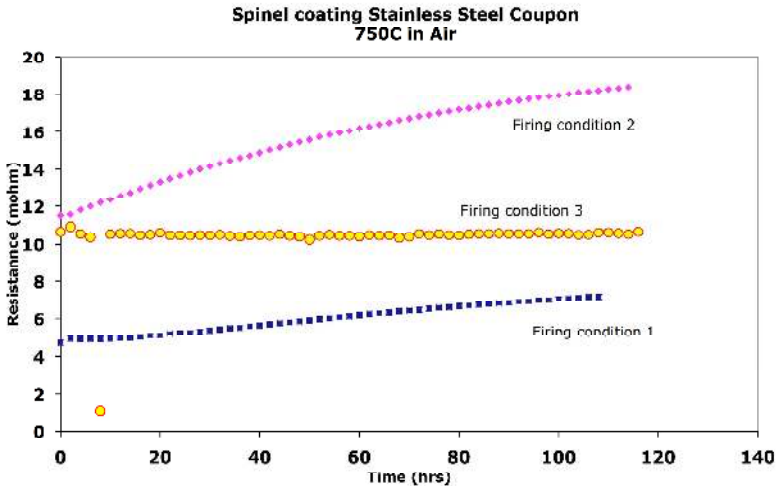

Figure 18. Resistance of stainless steel coupon couples with spinel coating.

Stack Test

A single repeat unit using coated interconnects and a 10 x 10 cm (~200 µm electrolyte) cell with Ni(Mg)O anode and LSCo cathode was tested at 700°C. The performance stability was very good, as shown in Figure 19. However, the initial performance relative to stacks with no spinel coating nearly 30% lower. Further investigations of the source of added resistance are needed.

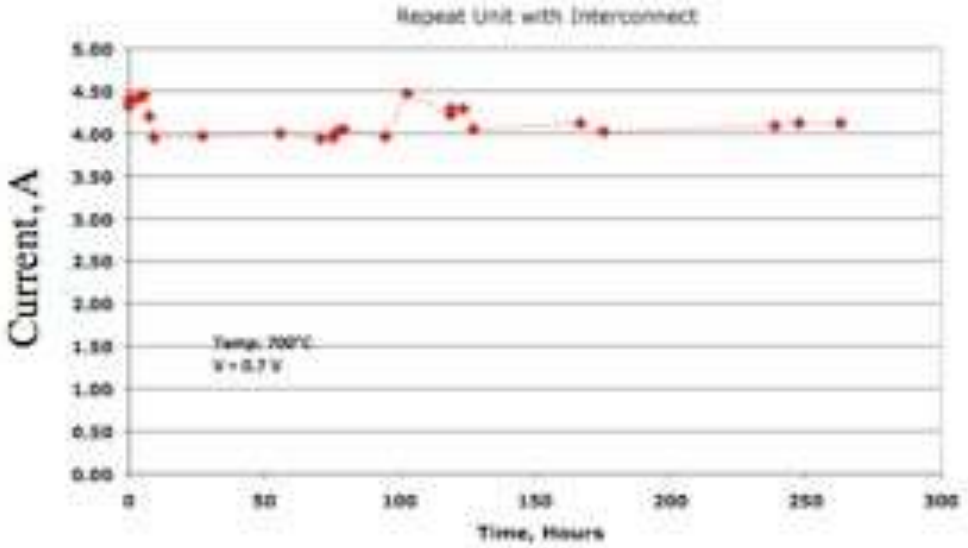

Figure 19. Stability of Gallate Repeat Unit

Conclusions

Lanthanum gallate electrolyte based SOFC offer the promise of high performance at the lower operating temperature. In this project, supported cell structure and cathode infiltration techniques were evaluated. Button cell performance showed encouraging results. However, more detailed analysis and experimental evaluation are needed to lower the in-plane resistance underneath the support structure. Limited evaluation was done on spinel coating of metal interconnects. The performance stability of stack repeat unit shows much needed improvement. However, additional resistance caused by the spinel treatment needs further investigation.

Alternative cathode compositions were evaluated at Northwestern University and CalTech. The results are summarized in the next two sections.

Chapter 3. Cathode Development at Northwestern University

A Study of $La_{0.9}Sr_{0.1}Ga_{0.8}Mg_{0.2}O_{3-\delta}$-$La_{0.6}Sr_{0.4}Fe_{0.8}Co_{0.2}O_{3-\delta}$ Composite Cathodes

Scott Barnett and Yuanbo Lin, Northwestern University

Introduction

We studied composite cathodes consisting of $La_{0.9}Sr_{0.1}Ga_{0.8}Mg_{0.2}O_{3-\delta}$ (LSGM) and $La_{0.6}Sr_{0.4}Fe_{0.8}Co_{0.2}O_{3-\delta}$ (LSCF), for use with LSGM-electrolyte SOFCs. Composition and processing conditions were varied and the resulting microstructure, electrochemical, and electrical properties were characterized (sections 2 and 3). Thin LSGM-electrolyte SOFCs were also fabricated to test the performance of the cathode (section 4). The CalTech cathode system was reproduced (section 5).

Experimental Procedure

Fabrication of Electrolyte Support Pellets

$La_{0.9}Sr_{0.1}Ga_{0.8}Mg_{0.2}O_{3-\delta}$ (LSGM) powder was prepared by solid-state reaction and die-pressed into pellets with diameter of 19 mm and thickness of about 0.5 mm under pressure of 10000 psi. The electrolyte pellets were sintered at 1450°C for 6 hours to achieve a dense structure.

Preparation of Symmetrical Cells

$La_{0.6}Sr_{0.4}$ $Co_{0.2}Fe_{0.8}O_{3-\delta}$ (LSCF, Praxair Inc.) powder was ball milled in ethanol with 30, 40, 50, 60 and 70wt% LSGM powder. Because the theoretical densities of LSGM (6.340g/cm^3, JCPDF card # 70-2788) and LSCF (6.426g/cm^3, JCPDF card # 89-5720) are very close to each other, the weight percentage of either phase can be taken as its volumetric percentage. In this study, the composition ranges for LSGM and LSCF were chosen to be from 30 to 70wt%, which is the within the percolation threshold for continuous pathway for both phases [1]. Nano-sized LSGM powder (Pechini method) from Ceramatec, Inc was also used in this study. Unless specifically indicated, LSGM-LSCF composite cathodes were made with solid-state reacted LSGM powder.

The milled powder mixture was dried, sieved with a 120# mesh screen, and made into an ink with V-737 screen-printing vehicle (Heraeus) in a powder-to-vehicle weight ratio of 50:50 by using a three-roll mill. The composite cathode paste was applied on both sides of the LSGM electrolyte pellets and fired at 1000-1300°C for 1 hour. Another layer of pure LSCF was applied on top of the composite cathode as a current collector layer, fired at 1000-1100°C for 1 hour. A current collector grid was applied on top of the cathodes with silver paste (DAD-87, Shanghai Research Institute of Synthetic Resin). The cell was mounted on an alumina tube with both sides exposed to ambient air. Silver wires were attached to the electrodes with two on each side for electrochemical characterization.

Electrochemical Characterization

The electrochemical tests were carried out by using a two-probe configuration under open circuit conditions, as shown in Fig. 1. The electrochemical impedance spectra (EIS) of the symmetrical cells were taken with an Electrochemical Workstation (IM6, ZAHNER) from 550 to 800°C. The frequency range for the impedance measurement was 0.1Hz to 1MHz and the signal

amplitude was 20mV. The cathode microstructure was observed after testing using scanning electron microscopy (SEM) in a Hitachi 3500 microscope. The electrical conductivities of the composite cathodes were tested using the van der Pauw method on samples with only LSGM-LSCF layer from 400 to 800°C.

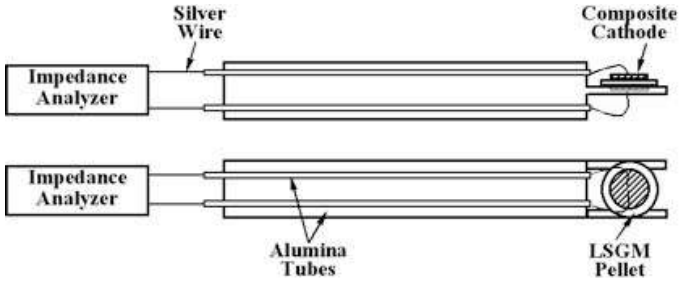

Figure 1 Schematic views of electrochemical impedance testing setup or symmetric cell EIS measurements. The upper one is a side view; lower one is a top view of the setup.

Results and Discussion

Chemical Compatibility of LSGM and LSCF

LSGM is chemically stable in a very narrow compositional region from the phase diagram [2]. Previous research has shown that resistive phases of $LaSrGaO_3$ and $LaSrGa_3O_7$ could result from the La enrichment or depletion in LSGM [3]. It is essential to ensure that the La chemical activity in LSCF is the same as that in LSGM to avoid low electrode performance from deleterious phases [3]. Initial tests were thus carried out to observe if there is any reaction between LSCF and LSGM. Figure 2 shows the XRD patterns of pure LSGM powder, pure LSCF powder, the mixture of 50wt% LSGM-50 wt% LSCF after ball milling, and the pellets from the mixture sintered at 1000-1200°C for 4 hours. Both LSCF and LSGM have perovskite structures. From the XRD patterns, no peaks corresponding to secondary phases (detection limit ~3%) were detected. These results indicate that LSGM and LSCF are chemically compatible, and that no La-ion diffusion occurs during preparation processes. Although there might be diffusion of Co or Fe into LSGM [4], this doping would only introduce electronic conduction in LSGM rather than producing resistive phases that decrease electrode performance [5-7].

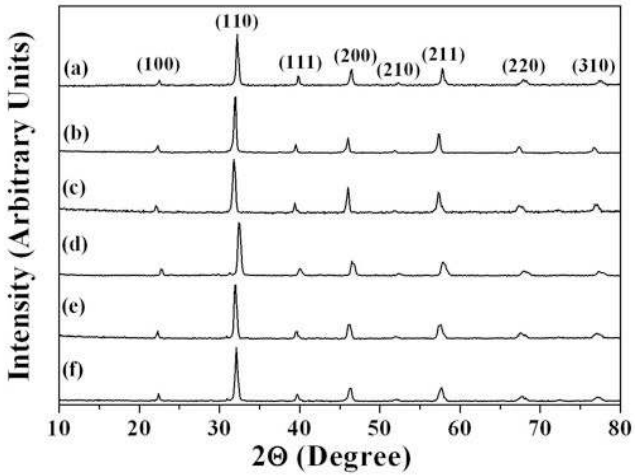

Figure 2 XRD patterns from (a) pure LSCF powder, (b) pure LSGM powder, mixture of LSCF and LSGM (50:50 wt%) (c) after ball milling, (d) after firing at 1000ºC for 4 hours, (e) 1100ºC for 4 hours, (f) 1200ºC for 4 hours. All peaks correspond to those for the perovskite structure.

Effect of Sintering Temperature

Figure 3(a)-(d) show the morphologies of cross-sectional SEM images of the composite cathodes (50wt% LSGM-50wt% LSCF) sintered at 1000-1300°C respectively. The LSGM substrate is at the bottom. In Fig. 3(a), two distinct phases of LSGM particles of sub-micron size and nano-size LSCF grains were presented in the composite cathode fired at 1000°C. The two components were not sintered well as indicated by poor mechanical strength, and the cathode was loosely bonded to the electrolyte pellet. At a temperature of 1100°C and above, the two phases were better sintered as indicated by better mechanical strength and good adhesion to the electrolyte. However, at elevated temperature of 1200°C and 1300°C, the cathodes showed larger grain sizes and less porosity, as shown in fig. 3(b)-(d).

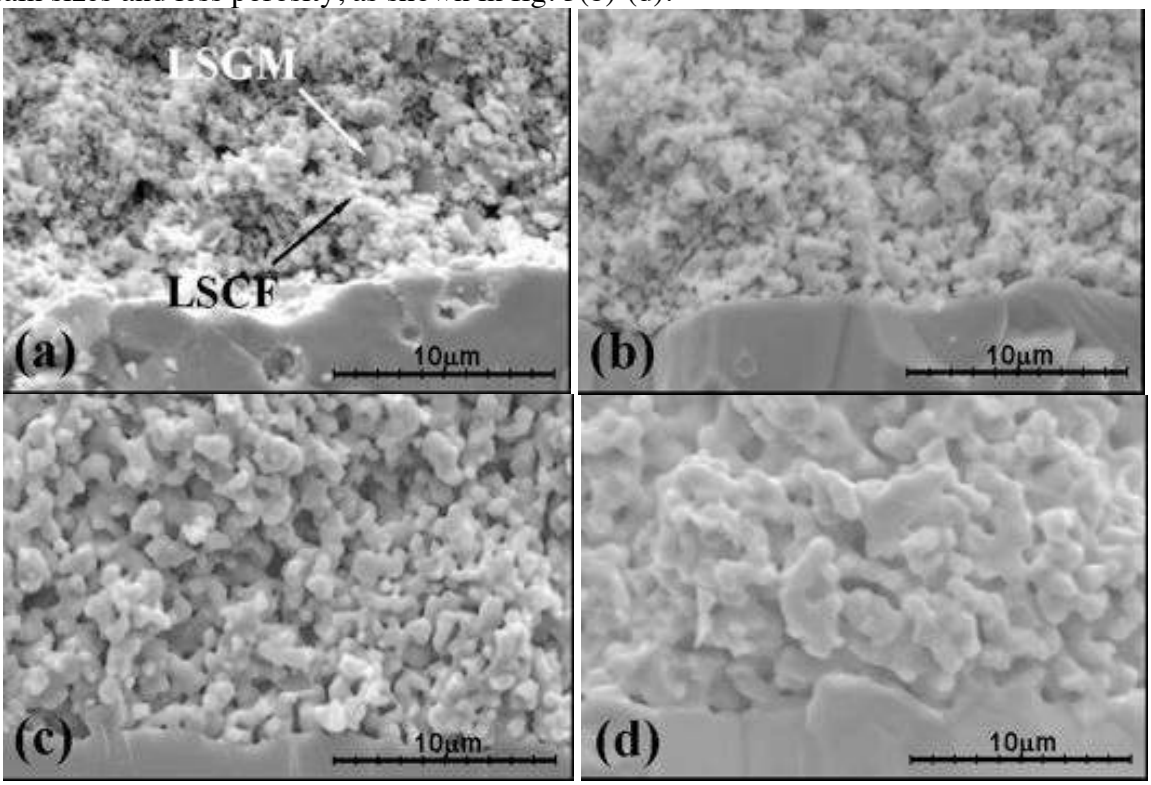

Figure 3 Cross-sectional SEM images of the composite cathodes (50wt% LSGM-50wt% LSCF) sintered for 1 h at (a) 1000, (b) 1100, (c) 1200 and (d) 1300ºC. The LSGM substrate is at the bottom.

Table 1 shows the total interfacial polarization area specific resistances, R_{AS} (i.e. the difference between the real axis intercepts of the impedance arcs) from electrochemical impedance measurements for the cathodes sintered at temperatures. The cathode sintered at 1100°C showed the lowest R_{AS} in the intermediate temperature range (550-700°C). For a given electrode composition, the weak minimum of the total R_{AS} as a function of firing temperature can be explained as a competition between two mechanisms. First, increasing firing temperature leads to larger grain sizes with correspondingly lower surface area; this is expected to increase the polarization resistance of mixed-conducting cathodes[8]. Porosity may also be reduced leading to possible concentration polarization. Second, the better connectivity between components (LSCF-LSGM, LSCF-LSCF, and LSGM-LSGM) at higher firing temperatures will tend to

reduce interfacial polarization. Collectively, the microstructural and electrochemical measurements gave the optimal sintering temperatures as 1100 to 1200°C.

Table 1 Summary of the total interfacial polarization resistances for the cathodes with 50wt% LSGM – 50wt% LSCF sintered at different temperatures. The electrochemical testing was taken at various temperatures from 550 to 800°C.

Temperature (°C)	Total Interfacial Polarization R_{AS} ($\Omega \cdot cm^2$)			
	$T_{Sintering}$=1000°C	$T_{Sintering}$=1100°C	$T_{Sintering}$=1200°C	$T_{Sintering}$=1300°C
550	4.6205	3.04773	3.11702	4.5541
600	0.90822	0.69045	0.6757	0.79302
650	0.24007	0.18723	0.18888	0.19555
700	0.07307	0.06085	0.0704	0.07325
750	0.02198	0.02454	0.02833	0.02853
800	0.00845	0.01203	0.01295	0.01459

Effect of Cathode Composition

Figure 4 illustrates the total R_{AS} for cathodes with different compositions tested in air at 600, 650 and 700°C. In general, the overall sizes of the impedance arcs were smaller for LSCF compositions from 40-60wt%. The lowest R_{AS} was found at 40wt%, *i.e.* 0.569, 0.181 and 0.0579 ($\Omega \cdot cm^2$) at 600, 650 and 700°C, respectively. However, at the same temperature, the impedance measurements showed no significant difference between samples with LSCF content from 40 to 60wt%. This suggests that the cathode composition was not the primary factor determining the electrochemical performance as long as similar contents of LSGM and LSCF were present. This is probably related to the good percolation of both phases expected in this composition range.

Figure 5 shows the temperature dependence of the total interfacial polarization resistance R_{AS} values for different LSCF-LSGM compositions. As discussed above, the R_{AS} values of different compositions are very close to each other, except for the case with 70wt% LSCF whose R_{AS} values are noticeably higher than others. However, the slopes of the log R_{AS} vs. 1/T data were nearly the same for all compositions, yielding an activation energy of 1.67±0.04 eV. This value is nearly identical to that of LSCF-GDC composite cathode reported previously [9], and in reasonable agreement with previous studies of LSCF cathodes whose activation energies are around 1.5eV [10,11].

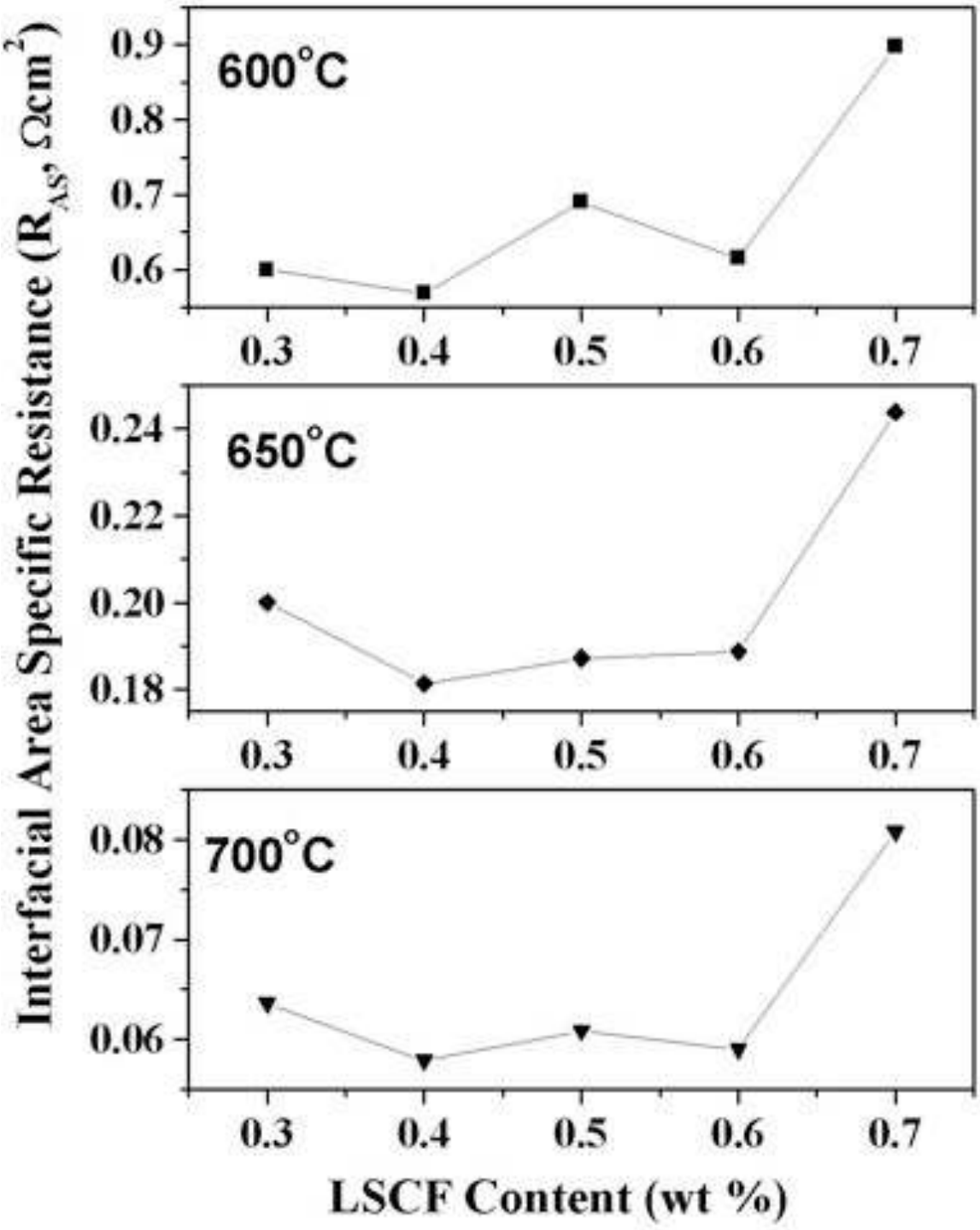

Figure 4 Total R_{AS} of composite cathodes as a function of LSCF content from 600 to 700ºC.

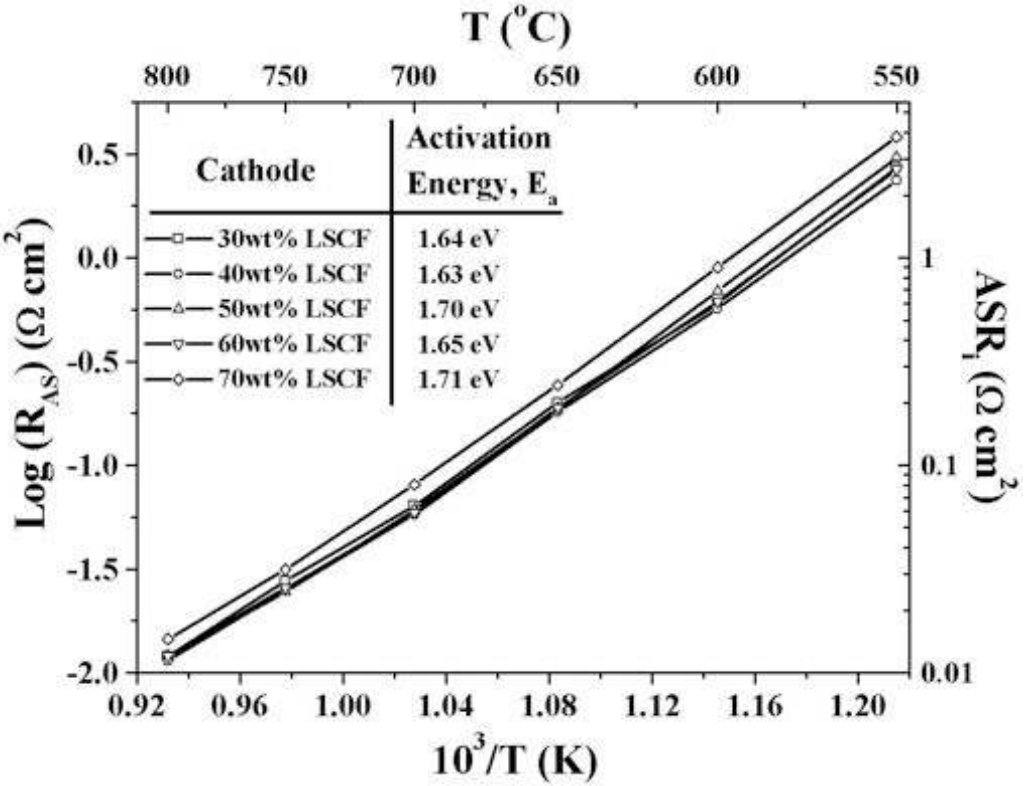

Figure 5. Temperature dependence of the total R_{AS} values for different LSCF-LSGM compositions measured over a temperature range of 550-800ºC in air under open circuit condition.

It is important to assure that the cathode retains good conductivity despite the addition of LSGM to LSCF. To measure the electrical conductivities of the composite cathodes with different compositions, only composite layers were applied on one side of LSGM pellets without additional LSCF layers. Figure 6 plots the DC electrical conductivity of different cathodes tested with the van der Pauw method [12] for temperatures from 400 to 800°C. Considering that the electrical conductivity from LSGM is low (0.10 S/cm at 800°C in air) [13], the major contribution to electrical conductivity is from the LSCF phase. At a given temperature, higher LSCF contents yield higher electrical conductivities, with the highest value of 34.6 S/cm at 800°C for 30wt% LSGM-70wt% LSCF. This trend may be attributed to the increase in the continuity of the electronically conductive LSCF phase in the porous composite. Pure dense LSCF was reported to have a high intrinsic electrical conductivity of 300-400 S/cm at 600°C for the composition in this study, i.e. $La_{0.6}Sr_{0.4}$ $Co_{0.2}Fe_{0.8}O_{3-\delta}$ [13,14]. The measured conductivity values were a factor of 10-100 lower than the above reported values (27.7 S/cm for 30wt% LSGM-70wt% LSCF and 1.90 S/cm for 70wt% LSGM-30wt% LSCF at 600°C). We believe that this was mainly due to the dilution effect of LSGM plus the porous structure of the composite. For a given composition, the electrical conductivity increases with temperature, which has been explained by the temperature-dependant conduction mechanisms of LSCF [15]. The conductivity of a thin (~25μm) electrode active layer with a current-collector layer (*e.g.* pure LSCF) should be > 1 S/cm for negligible performance loss (ohmic resistance ~ 0.0025 Ωcm^2). All of the composite cathode compositions thus had sufficient conductivity.

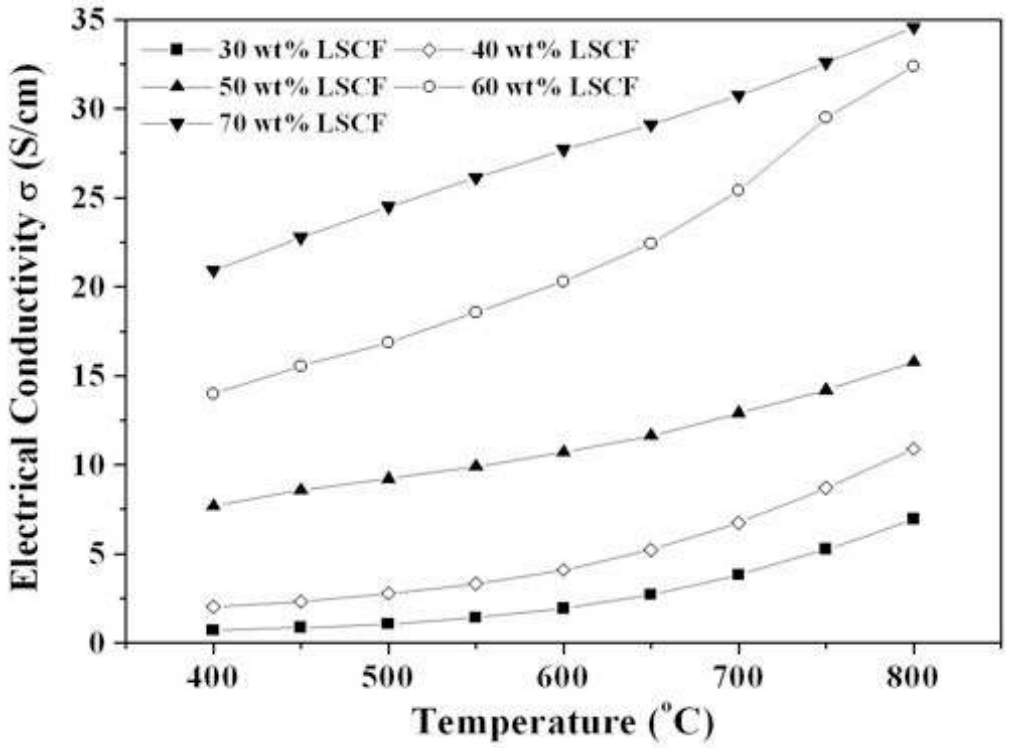

Figure 6 Plot of total conductivity versus temperatures for different cathode compositions.

Effect of Oxygen Partial Pressure

The oxygen partial pressure dependence of total R_{AS} values were measured at 600-800°C over an oxygen partial pressure range from 0.01 to 1 atm (Figure 7). Overall, a relatively weak oxygen partial pressure dependence for the cathodes with different compositions was observed, for example at 650°C, $R_{AS} \propto (PO_2)^{-0.204\pm0.035}$. This agrees with the usual power-law form of the resistance where an exponent m = 0 to 1/3 and an activation energy ≈ 1eV suggests that adsorption was the rate limiting mechanism [16], the same as for the composite cathodes systems reported previously [9,17].

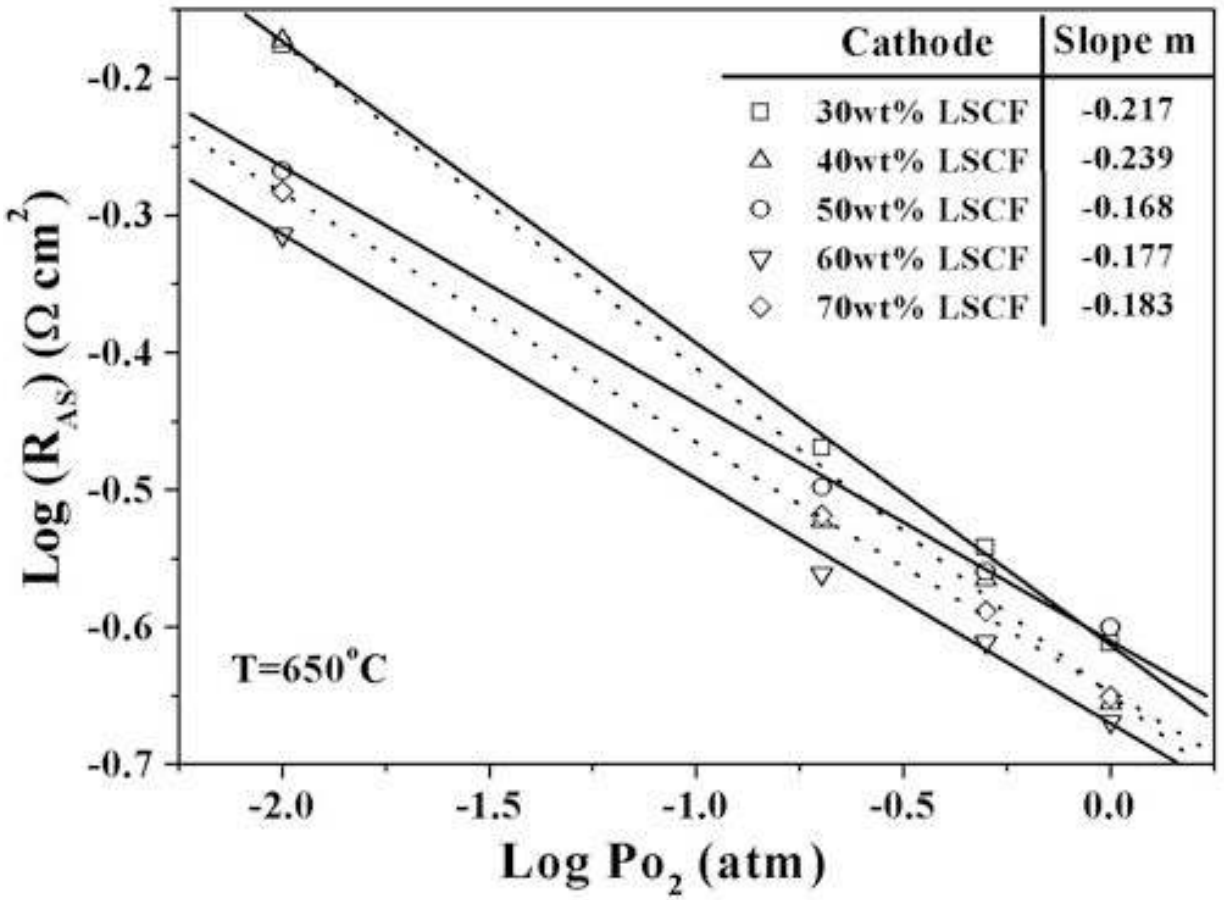

Figure 7 Total interfacial polarization resistance, R_{AS}, versus oxygen partial pressure for various LSCF-LSGM cathode compositions measured at 650°C.

Stability of LSCF-LSGM Composite Cathode

Figure 8 shows the R_{AS} of the cathode with 70 wt% LSCF- 30wt% LSGM under a constant current load of 0.5A/cm^2 at 650°C in air. Excellent stability was observed over the 700+ hour test, and also during a subsequent 400+ h of testing without an applied current. The result demonstrates that good stability can be achieved with LSGM-LSCF cathodes operated under realistic conditions.

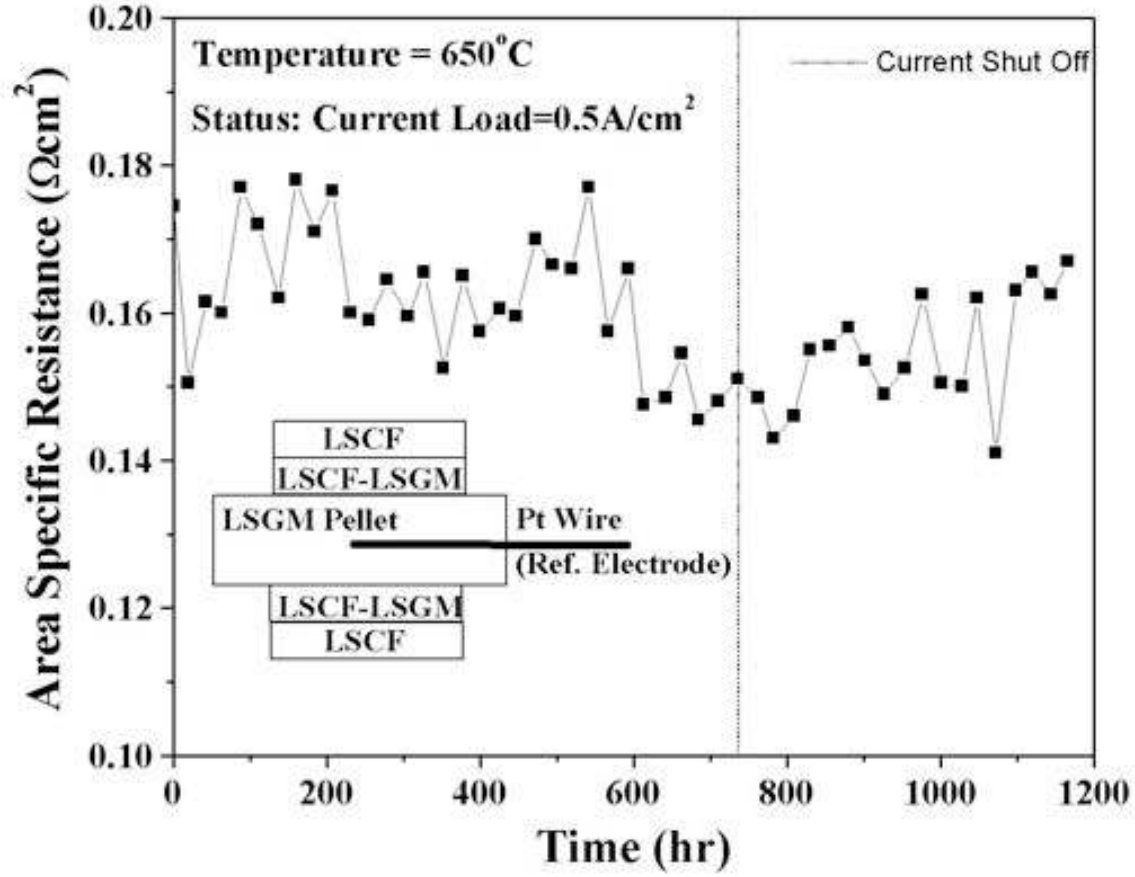

Figure 8. Long-term stability behavior of the cathode with 70 wt% LSCF- 30wt% LSGM under a constant current load of 0.5A/cm^2 at 650°C in air. The insert plot shows the symmetric cell under current load for the EIS measurements.

LSCF-LSGM composite cathode performance in an anode-supported SOFC

Introduction

Electrolyte-supported and thick film LSGM SOFCs have been fabricated and have shown excellent performance at 800ºC [18-20]. However, fabrication of thin electrode-supported LSGM layers [21,22] has proven challenging because of chemical reactions or ionic migration during high-temperature co-firing with electrodes. Indeed, the most successful thin-LSGM SOFCs were fabricated using a low temperature process, physical vapor deposition, to produce very thin Sm-doped Ceria (SDC) barrier layers between the LSGM and electrodes. In co-fired LSGM cells, however, a $(Ce_{0.6}La_{0.4})O_x$ (LDC) must be used to minimize reactions and interdiffusion between LSGM and the NiO-containing anode and the cathode. The 40% La content helps to maintain a constant La chemical potential in the electrolyte and barrier layers, thereby avoiding La out-diffusion from the LSGM layer [3,23,24]. Nonetheless, fabrication of thin-LSGM electrolyte SOFCs by co-firing has remained problematic.

In this chapter, we explored the use of co-firing to prepare anode-supported thin-LSGM electrolyte SOFCs with LDC interlayers. Dense thin LDC/LSGM/LDC layers on NiO-LDC anode substrates by co-sintering were demonstrated, with no evidence of deleterious reactions. SOFC testing yielded relatively high power densities but open-circuit voltages were lower than

expected, apparently due to Ni in the LSGM. Issues with this approach to thin-LSGM SOFCs are discussed.

Experimental Procedure

$La_{0.9}Sr_{0.1}Ga_{0.8}Mg_{0.2}O_{3-\delta}$ (LSGM) powder was prepared via solid-state reaction. Stoichiometric amounts of La_2O_3, $SrCO_3$, Ga_2O_3 and MgO were mixed in ethanol alcohol for 24 hrs. The slurry was dried and fired at 1250°C for 12hrs. $La_{0.4}Ce_{0.6}O_{2-\delta}$ (LDC) powder was also produced by solid-state reaction of La_2O_3 and CeO_2 after firing at 1250°C for 12hrs. After grinding and sieving with 200# mesh screen, the powders were studied with X-ray diffraction (XRD) in a diffractometer with Cu K_α radiation. The XRD patterns (Figure 6.1) were analyzed and determined with Jade 6.5 software. The results showed good agreement with expected peaks for LSGM and LDC [3,20], with no indication of second phases.

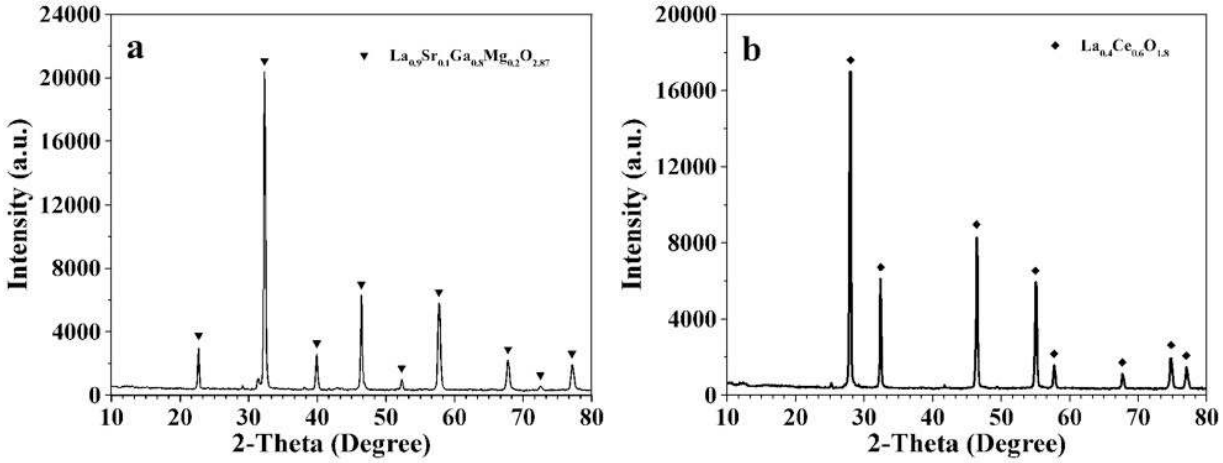

Figure 9. XRD patterns of (a) LSGM powder and (b) LDC powder prepared by solid-state reaction at 1250°C for 12hrs.

The Ni-LDC anode-supported fuel cells were prepared as follows. Commercial NiO (Alfa) and the above-described LDC powder with weight ratio 3:2 were ball milled together for 24hrs in ethanol with 10wt% starch as pore former and 0.5wt% polyvinyl butyral (PVB) as binder. The milled powder mixture was dried and pressed into pellets with diameter of 19 mm and thickness of about 0.6 mm. The pellets were bisque fired at 1100°C for 4 hours. LDC and LSGM colloidal suspensions were prepared by mixing the powder with binder and dispersant in ethanol. Layers of LDC, LSGM, and LDC were colloidally deposited sequentially on the anode support and the resulting green assembly was co-sintered at 1400°C for 4 hours. LDC and LSGM film thicknesses were controlled by the amount of colloidal solution applied onto the porous anode substrate. Cathodes consisting of a layer of 50wt% $La_{0.6}Sr_{0.4}Fe_{0.2}Co_{0.8}O_3$ (LSCF, Praxair) and 50wt% LSGM, followed by a pure LSCF layer, were applied on the electrolyte and fired at 1100°C for 1 hour.

The gas tightness of the LDC-LSGM-LDC composite layer was characterized with a vacuum measurement apparatus as previously described [25]. A smooth dense plate was used as a gas-tight reference sample.

SOFC single-cell tests were carried out using a standard geometry [26]. The anodes were reduced in humidified hydrogen at 600°C for 12 hrs. Current-voltage curves were then taken

from 550 to 750°C using an Electrochemical Workstation (IM6, ZAHNER), with the cathode exposed to ambient air and the anode to humidified (3% H_2O) hydrogen at a flow rate of 100 mL/min. The frequency range for the impedance measurement was 0.1Hz to 1MHz. The cell structure was observed after testing using scanning electron microscopy (SEM) in a Hitachi 3500 microscope.

Results and Discussion

Gas tightness measurements were carried out on the as-fired samples before application of the cathodes. Leakage was measured via the ultimate pressure achieved in a mechanically-pumped vacuum system with the SOFC sealed via a Viton o-ring. The SOFCs typically showed nearly the same ultimate steady pressure of the electrolyte membrane (50-100 mTorr) as that of the dense standard (50 mTorr). Previous measurements with YSZ thin electrolytes, that subsequently yielded near-ideal open circuit voltages during cell test, yielded similar results [25]. These results indicate that dense composite electrolyte layers were obtained with this method.

Figure 10 shows an example of a cross-sectional SEM image of the LDC/LSGM/LDC tri-layer along with the surrounding anode and cathode materials. The LDC and LSGM layers were uniform in thickness without cross-membrane pinholes or cracks and appeared to have only a small amount of porosity. There was good intimate contact between the LSGM and LDC layers and the surrounding electrodes, showing that the materials sintered well together. The LSGM layer was ≈ 9μm thick and the LDC layers were ≈ 7-10 μm thick.

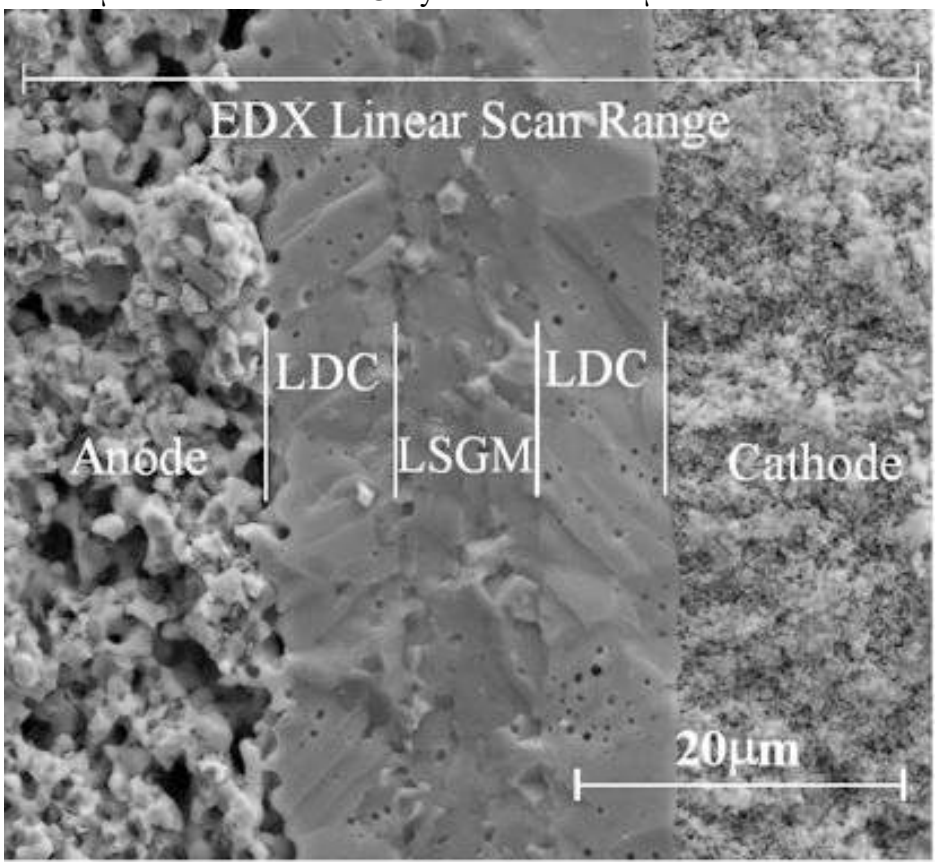

Figure 10. Cross-sectional SEM image of a typical LDC/LSGM/LDC electrolyte tri-layer and also showing portions of the Ni-LDC anode support and LSGM-LSCF/LSCF cathode.

Figure 11 illustrates typical cell performance. The peak power densities were 1.12, 0.91, 0.60, 0.33 and 0.17 W/cm^2, at 750, 700, 650, 600 and 550ºC, respectively. These power densities are comparable to the best previously reported values for thick-film or electrolyte-supported LSGM SOFCs (e.g. 0.4-0.6 W/cm^2 at 700ºC) [3,18-20]. In one case where much higher LSGM power densities were reported [21,22], LSGM and Sm-doped Ceria interlayers were deposited at relatively low temperature using pulsed laser deposition (avoiding possible reaction/diffusion problems), and the testing was done with pure oxygen at the cathode. The open circuit voltage (OCV) was 0.98V at 650ºC, lower than that of a thick LSGM film single cell (above 1.1V) on H_2 and air [3]. This was presumably not due to gas leakage across the electrolyte, based on the relatively dense appearance of the layers (Figure 6.2), low measured gas leakage rates, and the observation that the OCV did not fluctuate with changes in gas flow rates. The low OCV can alternatively be explained by the diffusion of transition metal cations (e.g. Co, Fe, Ni) from electrodes into LSGM layer during sintering. Although low concentrations of transition metal cations in LSGM improves the oxide ion conductivity without the significantly decreasing the oxide-ion transference number [27,28], larger concentrations cause significant hole conduction and reduce OCV [5-7].

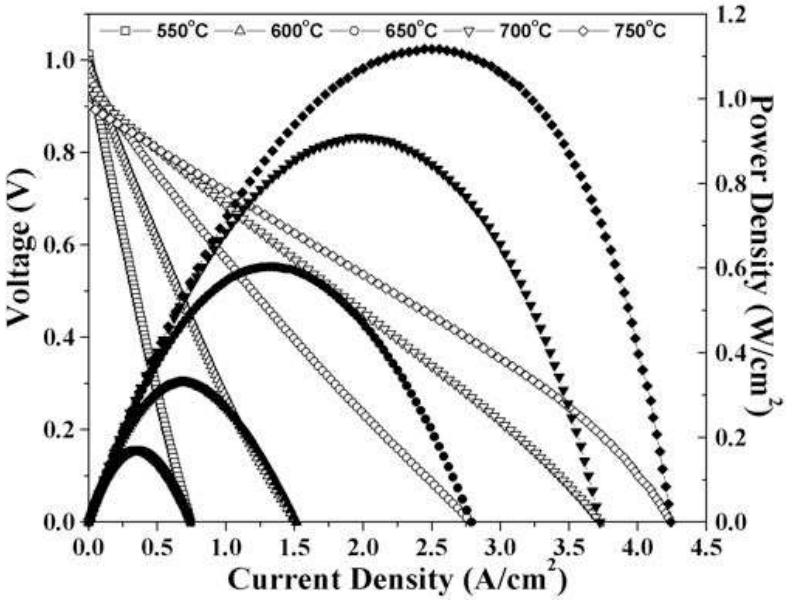

Figure 11. Voltage and power density vs. current density of a thin-LSGM SOFC operated on air and humidified hydrogen with a flow rate of 100 mL/min.

Figure 12 shows the results of EDX linear scans for transition elements (Co, Fe, Ni) across the cross sectional area shown in Fig. 10. It was observed that the LDC buffer layer between cathode and electrolyte successfully blocked the diffusion of Fe and Co cations from the cathode into the LSGM film, probably because of the relatively low cathode firing temperature. However, obvious Ni peaks were seen in the LSGM film, presumably due to diffusion during the prolonged high temperature co-firing. These results strongly suggest that the Ni-induced hole conduction resulted in the low OCV.

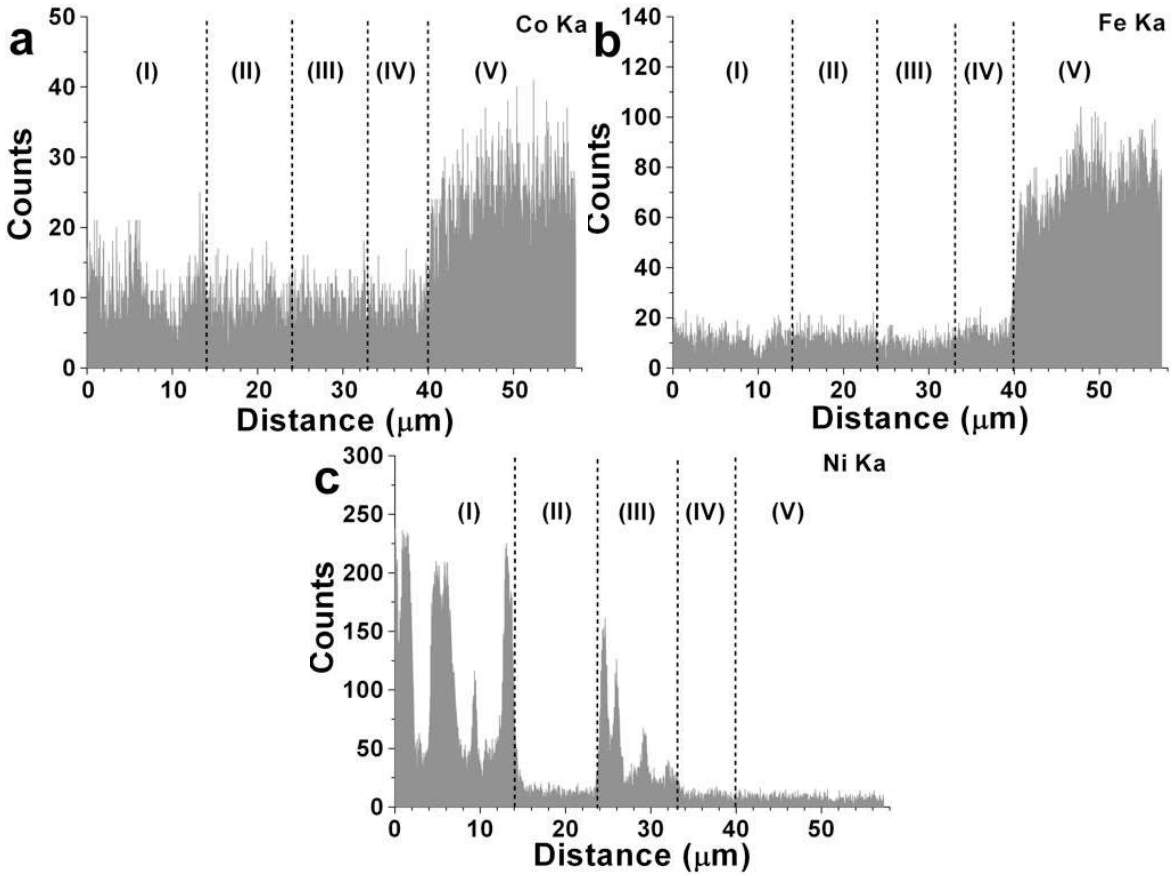

Figure 12. EDX linear scans of (a) Co, (b) Fe and (c) Ni peak intensities across the (I) Ni-LDC anode, (II) LDC buffer layer, (III) LSGM electrolyte, (IV) LDC buffer layer, and (V) LSCF-LSGM cathode.

Electrochemical impedance spectra from the cell in Figure 11 are shown in Figure 13. Figure 13 indicates that the ohmic electrolyte resistance contribution was comparable to that of the electrodes. The relatively low total resistance and good cell performance show that the LDC buffer layers successfully prohibited the formation of high resistance phases, e.g. $LaSrGa_3O_7$ due to La-depletion, or reaction products between LSGM and the electrodes, e.g. $LaNiO_3$ [3]. The high-frequency real-axis intercepts on Nyquist impedance plots give the total cell ohmic resistance R, which arises primarily from the electrolyte and interlayers (previous experience with this single cell test apparatus suggests that electrodes, contacts, and connecting wires were a relatively small contribution).

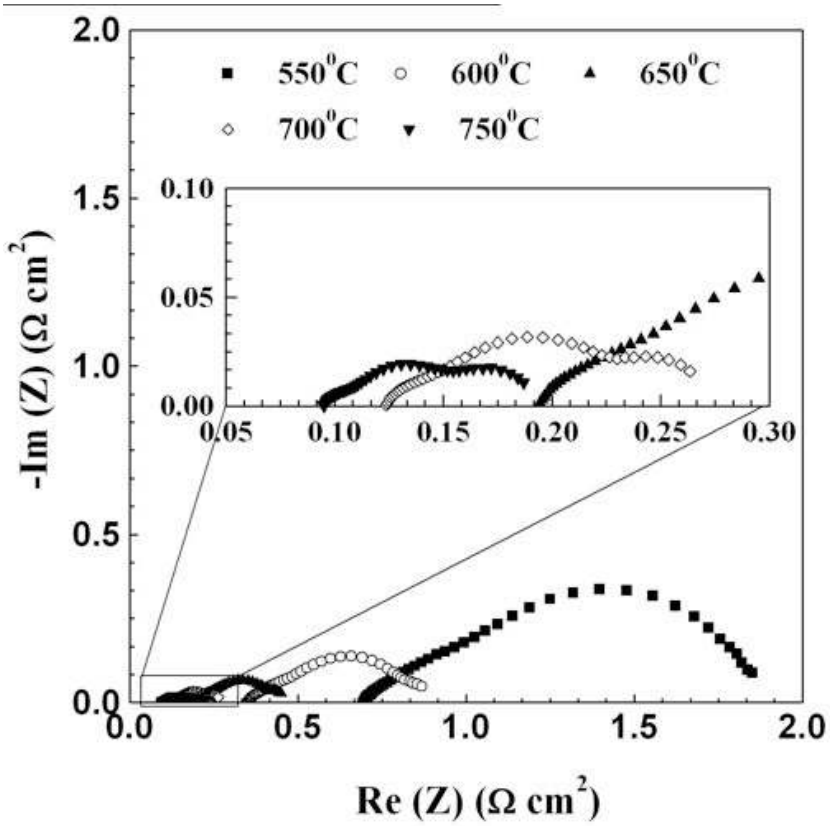

Figure 13. Electrochemical impedance spectra from a thin-LSGM SOFC measured at open-circuit potential in air and humidified hydrogen.

The total ohmic resistance values acquired from the impedance spectra are plotted versus temperature T in Figure 14, along with expected ohmic resistances for 10-μm-thick YSZ and LSGM calculated using reported conductivity values [29]. The measured electrolyte resistance was lower than expected for YSZ, but higher than expected for LSGM. The difference from the calculated LSGM electrolyte was clearly due to the LDC interlayers. Based on the difference between the measured composite electrolyte resistance and that of LSGM, we conclude that the resistivity of LDC was ~63 Ωcm at 700ºC. Resistivity values for such heavily doped LDC have not been reported to our knowledge. However, the ionic resistivity value of $La_{0.2}Ce_{0.8}O_{1.9}$ at 700ºC was reported to be ~24 Ωcm [30]. While this is lower than the present value for $La_{0.4}Ce_{0.6}O_{1.8}$, the conductivity of doped ceria generally decreases with increasing dopant concentration over 20atm% (see Ref [31] for typical results for Sm-doped Ceria). The present value is thus consistent with prior conductivity data. Another conclusion from Figure 14 is that the good cell performance, compared to thin-YSZ electrolyte cells, was due to low polarization resistance rather than low electrolyte resistance. This may be attributed to a low polarization resistance for electrodes in contact with LDC versus YSZ [32].

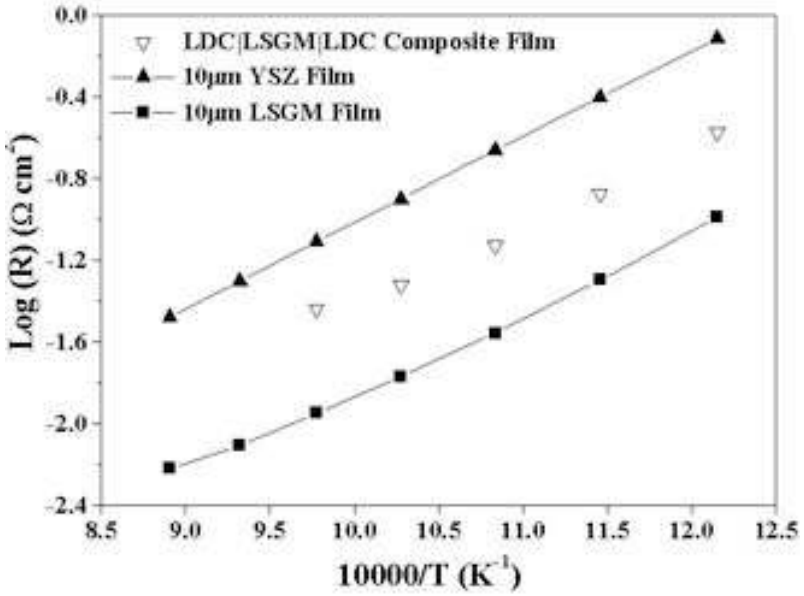

Figure 14. Total ohmic resistance R vs. 10000/T for a thin-LSGM SOFC. Shown for comparison are the calculated ohmic resistances of YSZ and LSGM thin films [29].

While the present results show that good LSGM-electrolyte anode-supported SOFCs can be made with co-firing, it is clear that the use of LDC inter-layers involves trade-offs. While the LDC minimizes reactions/interdiffusion between LSGM and the electrodes, it substantially increases the total resistance. Improvements will be needed in order to achieve lower electrolyte resistance, and hence, better low-temperature performance than YSZ electrolyte cells. It may be possible to reduce the cathode LDC layer thickness, since no Co or Fe were found in the electrolyte. The LSGM layer thickness could also be decreased slightly to help reduce the electrolyte resistance. On the other hand, it will be difficult to reduce the anode LDC layer thickness because this would increase Ni diffusion into the LSGM layer, further reducing the OCV. An alternate approach would be to alter the LDC composition, e.g. by adding another dopant, in order to increase its conductivity closer to that for Sm-doped or Gd-doped Ceria [33,34]. Finally, a reduced co-firing temperature, but still high enough to achieve a dense LSGM electrolyte, may be useful to reduce Ni diffusion even for relatively thin inter-layers.

Testing of CalTech Cathode Materials

In order to provide an independent confirmation of the results for BSCF cathodes at CalTech, we carried out symmetrical sample fabrication and testing at Northwestern University. While the colloidal materials were obtained from CalTech, the remainder of the fabrication process, including electrolyte and electrode fabrication, were done at Northwestern University. The goal of this work was to verify that both the EIS measurements and the fabrication processes could be readily reproduced. This was achieved in a single experiment, as we were able to reproduce the CalTech electrochemical test results on a sample that we prepared.

The symmetrical cell BSCF cathode was prepared by starting with an LSGM pellet, prepared as described above. The BSCF layers were prepared by drop-coating 8 μl of the colloidal suspension onto the LSGM pellet surface. The drop coat was repeated identically on

both sides of the pellet, and then the pellet with electrodes fired at 820°C for 5hr (this was the preferred condition from CalTech). Finally, 10 µl of the CalTech Ag-Si current collector suspension was drop coated onto the cathode surfaces on both sides, and then fired at 700°C for1hr.

Figure 15 shows a typical EIS result obtained at 650°C in air. The spectrum shows a single depressed arc corresponding to the cathode polarization resistance. Note that the results have already been normalized to the electrode area and divided by two to give a value for a single cathode relevant to a SOFC. Fitting of the arcs was not done, but the polarization resistance was estimated from the real-axis intercepts of the arcs. The value at 650C is ~0.6 Ωcm^2, in reasonable agreement with the value reported by CalTech. Table 2 gives the estimated polarization resistance values at selected temperatures. The resistance is quite low even down to 600°C, showing that BSCF is a promising low-temperature cathode material.

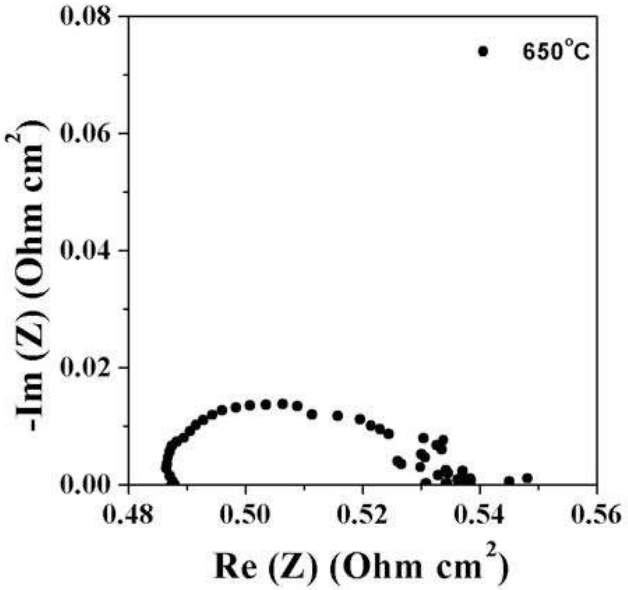

Figure 15. Example of EIS data from a symmetrical BSCF cathode sample on a LSGM electrolyte.

Table 2. Cathode polarization resistance values at different measurement temperatures estimated from the EIS arc real-axis intercepts.

Temperature (°C)	Interfacial Area Specific Resistance (Ωcm^2)
525	~0.8
550	~0.5
575	~0.25
600	~0.15
625	~0.1
650	~0.06
675	~0.03

Summary and Conclusions

LSCF-LSGM composite cathodes were investigated. The optimum sintering temperature was 1100 - 1200°C. LSCF content between 40-60wt% gave the best electrochemical performance. The oxygen partial pressure dependence of the composite cathodes was relatively weak. The composite cathode performance was stable under a current load for >600h at 650°C. The polarization resistance was < 0.2 Ωcm^2 at 650°C in air. These results show that LSCF-LSGM is a promising cathode materials for intermediate-temperature LSGM-electrolyte SOFCs, with good stability and a wide range of processing parameters that yield good properties.

Anode-supported SOFCs with dense thin LDC/LSGM/LDC electrolytes were fabricated by co-sintering. Maximum power densities were 1.12W/cm^2, 0.91W/cm^2 and 0.60W/cm^2 at 750°C, 700°C and 650°C, respectively. The good performance and low ohmic resistance suggests that there was no significant formation of interfacial phases. The results indicate a trade-off regarding the thicknesses of the LDC barrier layers: reducing the LDC thickness would be useful for reducing ohmic resistance but would also increase in-diffusion of impurities such as Ni into the LSGM electrolyte. The situation could be improved if co-firing temperatures and/or times could be reduced, or a more conductive barrier layer composition used. Finally, the impedance measurements show that improved electrodes are needed to achieve really good low-temperature performance.

Finally, our experiments successfully reproduced the cathode electrochemical test results for the BSCF cathode developed at CalTech.

References

1. Minh, N.Q., Ceramic Fuel Cells. *J. Am. Ceram. Soc.* **76**(3), 563-588 (1993).
2. Huang, P.-N. & Petric, A., Superior Oxygen Ion Conductivity of Lanthanum Gallate Doped with Strontium and Magnesium. *J. Electrochem. Soc.* **143**(5), 1644-1648 (1996).
3. Huang, K., Wan, J.-H. & Goodenough, J.B., Increasing Power Density of LSGM-Based Solid Oxide Fuel Cells Using New Anode Materials. *J. Electrochem. Soc.* **148**(7), A788-A794 (2001).
4. Naoumidis, A., Ahmad-Khanlou, A., Samardzija, Z. & Kolar, D., Chemical interaction and diffusion on interface cathode/electrolyte of SOFC. *Fresenius Journal of Analytical Chemistry* **365**(1-3), 277-281 (1999).
5. Ishihara, T., Shibayama, T., Nishiguchi, H. & Takita, Y., Oxide ion conductivity in $La_{0.8}Sr_{0.2}Ga_{0.8}Mg_{0.2-X}Ni_XO_3$ perovskite oxide and application for the electrolyte of solid oxide fuel cells. *J. Mater. Sci.* **36**(5), 1125-1131 (2001).
6. Ishihara, T., Shibayama, T., Honda, M., Nishiguchi, H. & Takita, Y., Intermediate Temperature Solid Oxide Fuel Cells Using $LaGaO_3$ Electrolyte II. Improvement of Oxide Ion Conductivity and Power Density by Doping Fe for Ga Site of $LaGaO_3$. *J. Electrochem. Soc.* **147**(4), 1332-1337 (2000).
7. Ishihara, T., Shibayama, T., Honda, M., Nishiguchi, H. & Takita, Y., Solid oxide fuel cell using Co doped La(Sr)Ga(Mg)O_3 perovskite oxide with notably high power density at intermediate temperature. *Chem. Commun.* **13**, 1227-1228 (1999).
8. Adler, S.B., Lane, J.A. & Steele, B.C.H., Electrode Kinetics of Porous Mixed-Conducting Oxygen Electrodes. *J. Electrochem. Soc.* **143**(11), 3554-3564 (1996).

9. Murray, E.P., Sever, M.J. & Barnett, S.A., Electrochemical performance of (La,Sr)(Co,Fe)O_3-(Ce, Gd)O_3 composite cathodes. *Solid State Ionics* **148**(1-2), 27-34 (2002).
10. Waller, D., Lane, J.A., Kilner, J.A. & Steele, B.C.H., The effect of thermal treatment on the resistance of LSCF electrodes on gadolinia doped ceria electrolytes. *Solid State Ionics* **86-88**(2), 767-772 (1996).
11. Dusastre, V. & Kilner, J.A., Optimisation of composite cathodes for intermediate temperature SOFC applications. *Solid State Ionics* **126**(1-2), 163-174 (1999).
12. Pauw, L.J.v.d., A method of measuring specific resistivity and Hall effect of discs of arbitrary shape. *Philips Research Reports* **13**(1), 1-9 (1958).
13. Ullmann, H., Trofimenko, N., Tietz, F., Stöver, D. & Ahmad-Khanlou, A., Correlation between thermal expansion and oxide ion transport in mixed conducting perovskite-type oxides for SOFC. *Solid State Ionics* **138**(1-2), 79-90 (2000).
14. Tai, L.-W., Nasrallah, M.M., Anderson, H.U., Sparlin, D.M. & Sehlin, S.R., Structure and electrical properties of $La_{1-x}Sr_xCo_{1-y}Fe_yO_3$. Part 2. The system $La_{1-x}Sr_xCo_{0.2}Fe_{0.8}O_3$. *Solid State Ionics* **76**(3-4), 273-283 (1995).
15. Esquirol, A., Brandon, N.P., Kilner, J.A. & Mogensen, M., Electrochemical Characterization of $La_{0.6}Sr_{0.4}Co_{0.2}Fe_{0.8}O_3$ Cathodes for Intermediate-Temperature SOFCs *J. Electrochem. Soc.* **151**(11), A1847-A1855 (2004).
16. Herle, J.V., McEvoy, A.J. & Thampi, K.R., A study on the $La_{1-x}Sr_xMnO_3$ oxygen cathode. *Electrochimica Acta* **41**(9), 1447-1454 (1996).
17. Murray, E.P. & Barnett, S.A., (La,Sr)MnO_3-(Ce,Gd)O_{2-x} composite cathodes for solid oxide fuel cells. *Solid State Ionics* **143**(3-4), 265-273 (2001).
18. Bi, Z., Yi, B., Wang, Z., Dong, Y., Wu, H., She, Y. & Cheng, M., A High-Performance Anode-Supported SOFC with LDC-LSGM Bilayer Electrolytes. *Electrochem. Solid-State Lett.* **7**(5), A105-A107 (2004).
19. Wan, J.-H., Yan, J.-Q. & Goodenough, J.B., LSGM-Based Solid Oxide Fuel Cell with 1.4 W/cm^2 Power Density and 30 Day Long-Term Stability. *J. Electrochem. Soc.* **152**(8), A1511-A1515 (2005).
20. Bi, Z., Cheng, M., Dong, Y., Wu, H., She, Y. & Yi, B., Electrochemical evaluation of $La_{0.6}Sr_{0.4}CoO_3$-$La_{0.45}Ce_{0.55}O_2$ composite cathodes for anode-supported $La_{0.45}Ce_{0.55}O_2$-$La_{0.9}Sr_{0.1}Ga_{0.8}Mg_{0.2}O_{2.85}$ bilayer electrolyte solid oxide fuel cells. *Solid State Ionics* **176**(7-8), 655-661 (2005).
21. Yan, J., Matsumoto, H., Enoki, M. & Ishihara, T., High-Power SOFC Using $La_{0.9}Sr_{0.1}Ga_{0.8}Mg_{0.2}O_{3-deta}$/$Ce_{0.8}Sm_{0.2}O_2$ Composite Film. *Electrochem. Solid-State Lett.* **8**(8), A389-A391 (2005).
22. Yan, J.W., Lu, Z.G., Jiang, Y., Dong, Y.L., Yu, C.Y. & Li, W.Z., Fabrication and Testing of a Doped Lanthanum Gallate Electrolyte Thin-Film Solid Oxide Fuel Cell. *J. Electrochem. Soc.* **149**(9), A1132-A1135 (2002).
23. Feng, M., Goodenough, J.B., Huang, K. & Milliken, C., Fuel cells with doped lanthanum gallate electrolyte. *J. Power Sources* **63**(1), 47-51 (1996).
24. Huang, K., Tichy, R.S. & Goodenough, J.B., Superior Perovskite Oxide-Ion Conductor; Strontium- and Magnesium-Doped $LaGaO_3$: I, Phase Relationships and Electrical Properties. *J. Am. Cer. Soc.* **81**(10), 2565-2575 (1996).
25. VonDollen, P. & Barnett, S.A., A Study of Screen Printed Yttria-Stabilized Zirconia Layers for Solid Oxide Fuel Cells. *J. Am. Cer. Soc.* **88**(12), 3361-3368 (2005).

26. Lin, Y., Zhan, Z., Liu, J. & Barnett, S.A., Direct operation of solid oxide fuel cells with methane fuel. *Solid State Ionics* **176**(23-24), 1827-1835 (2005).
27. Ishihara, T., Furutani, H., Honda, M., Yamada, T., Shibayama, T., Akbay, T., Sakai, N., Yokokawa, H. & Takita, Y., Improved oxide ion conductivity in $La_{0.8}Sr_{0.2}Ga_{0.8}Mg_{0.2}O_3$ by doping Co. *Chem. Mater.* **11**(8), 2081-2088 (1999).
28. Kharton, V.V., Viskup, A.P., Yaremchenko, A.A., Baker, R.T., Gharbage, B., Mather, G.C., Figueiredo, F.M., Naumovich, E.N. & Marques, F.M.B., Ionic conductivity of La(Sr)Ga(Mg,M)$O_{3-\delta}$ (M=Ti, Cr, Fe, Co, Ni): effects of transition metal dopants. *Solid State Ionics* **132**(1-2), 119-130 (2000).
29. Ishihara, T., Arikawa, H., Akbay, T., Nishiguchi, H. & Takita, Y., Nonstoichiometric La2-xGeO5-delta monoclinic oxide as a new fast oxide ion conductor. *J. Am. Chem. Soc.* **123**(2), 203-209 (2001).
30. Shimonosono, T., Hirata, Y., Sameshima, S. & Horita, T., Electronic Conductivity of La-Doped Ceria Ceramics. *J. Am. Cer. Soc.* **88**(8), 2114-2120 (2005).
31. Jung, G.-B., Huang, T.-J. & Chang, C.-L., Effect of temperature and dopant concentration on the conductivity of samaria-doped ceria electrolyte. *J. Solid State Electrochem.* **6**(4), 225-230 (2002).
32. Tsai, T. & Barnett, S.A., Increased solid-oxide fuel cell power density using interfacial ceria layers. *Solid State Ionics* **98**(3-4), 191-196 (1997).
33. Yoshida, H., Deguchi, H., Miura, K., Horiuchi, M. & Inagaki, T., Investigation of the relationship between the ionic conductivity and the local structures of singly and doubly doped ceria compounds using EXAFS measurement. *Solid State Ionics* **140**(3-4), 191-199 (2001).
34. Mori, T., Drennan, J., Lee, J.-H., Li, J.-G. & Ikegami, T., Oxide ionic conductivity and microstructures of Sm- or La-doped CeO_2-based systems. *Solid State Ionics* **154-155**, 461-466 (2002).

Chapter 4. Cathode Development at CalTech

Introduction

This report documents studies of the compatability and suitability of the high-activity cathode material, $Ba_{0.5}Sr_{0.5}Co_{0.8}Fe_{0.2}O_{3-\delta}$ or BSCF, to the high-conductivity electrolyte material, LSGM. The objective is to capitalize on the excellent transport properties of each of these components so as to develop exceptionally high power density SOFCs operating in the 500-800°C temperature range. We discuss in particular the interplay between LSGM powder synthesis, BSCF deposition, and electrochemical performance. In addition, a comparison to LSCF based cathodes is presented.

Sample Preparation and Phase Characterization

$La_{0.9}Sr_{0.1}Mg_{0.2}Ga_{0.8}O_{2.85}$ (LSGM) powder was provided by Ceramatec, and additional material prepared in-house by solid state reaction of the precursors La_2O_3, $SrCO_3$, MgO, and Ga_2O_3. Stoichiometric amounts of these powders were suspended in ethanol and stirred without heating for 24 hours. The ethanol was then removed by evaporation at 100°C and the powders calcined at 1375 °C for 16 hours under stagnant air. This step was followed by ball-milling to obtain powders < 106 μm. Successive heating and ball-milling were repeated until single-phase powders were obtained (typically three times). Preparation of dense LSGM pellets for electrochemical characterization is described below. In addition, thin LSGM discs (15.8 mm in diameter × 0.45 mm in thickness and 98% theoretical density) were supplied by Prof. Scott Barnett (Northwestern University). [SDC powders were obtained commercially from Nextech Materials (Nano Grade, surface area 204 m^2/g) and pressed into pellets under the same pressure and similar dimensions. Sintering was performed at 1350 °C]

BSCF was synthesized from its component metal nitrates using the EDTA-citric acid method as described elsewhere [1]. In brief, the nitrates ($BaNO_3$, $SrNO_3$, $CoNO_3$, and $FeNO_3$) were dissolved in water along with the complexing agents EDTA and citric. Mild heating induced gelation of the solution, and the resulting gel was held at 250 °C for 12 h to remove organics, and then calcined for 5 h under stagnant air at 900–1,050 °C. In addition to the desired stoichiometry of $Ba_{0.5}Sr_{0.5}Co_{0.8}Fe_{0.2}O_{3-\delta}$, samples with composition $Ba_{0.45}Sr_{0.45}La_{0.1}Co_{0.72}Fe_{0.18}Ga_{0.1}O_{3-\delta}$ (BSLCFG) were also prepared in order to probe the consequences of possible incorporation of La and Ga, the major elements of LSGM, into BSCF. Powder preparation proceeded in an analogous manner to synthesis of the standard material, with the addition of appropriate quantities of $LaNO_3$ and $GaNO_3$ into the starting solution. The relative ratios of Ba:Sr and Co:Fe in BSLCFG have been maintained relative to the original BSCF composition, and the A-site and B-site have been doped to 0.1 stoichiometry with La^{3+} or Ga^{3+} cations, respectively.

X-ray powder diffraction patterns obtained from these syntheses are shown in Figure 1 (CuKa radiation, X'Pert Pro diffractometer, 0.02 ° step size, 3 s dwell time). The LSGM patterns (Fig. 1a) reveal peaks due to one or more impurity phases in the Ceramatec material, whereas the Northwestern and Caltech LSGM are free of these of these extra peaks. The BSCF patterns (Fig. 1b) show that BSLCFG does not form a single cubic phase; several impurity peaks occur in this pattern relative to BSCF. However, the lattice constant of the majority perovskite phase in the BSLCFG material, 3.9540(4) Å, is slightly smaller than that of BSCF, 3.9865(1) Å, consistent with the incorporation of La and Ga into the structure. Thus, these elements might be expected to eventually be incorporated into the cathode material after long periods of fuel cell operation.

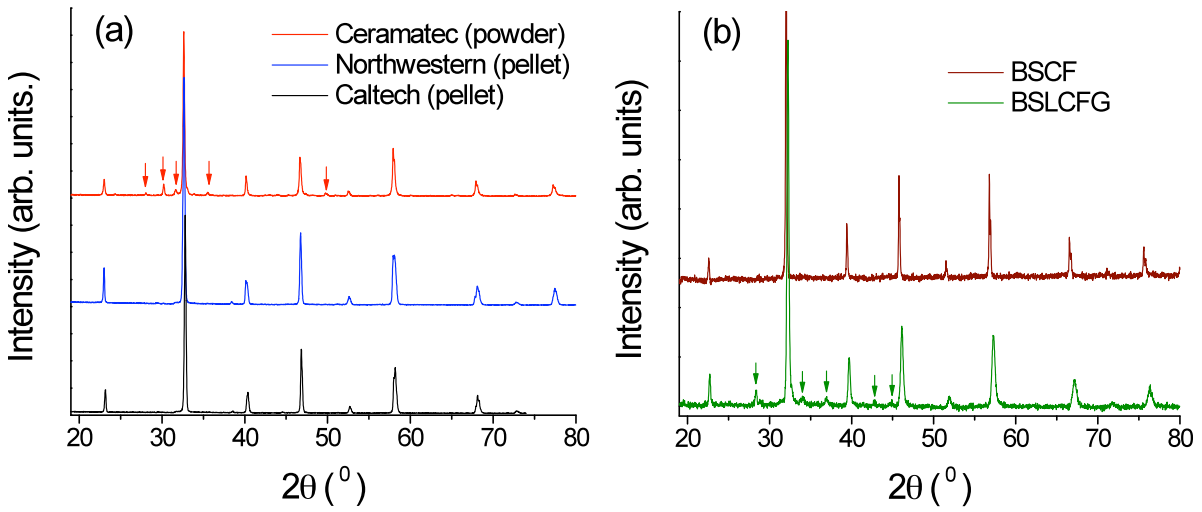

Fig. 1. X-ray powder diffraction patterns of (a) Ceramatec, Northwestern and Caltech LSGM; and (b) BSCF and BSLCFG.

The possibility of high temperature reactions between BSCF and LSGM was probed using *in situ* high temperature X-ray diffraction. In the case of LSGM provided by Ceramatek or synthesized in house at Caltech, mixtures of mixtures of BSCF and LSGM powders (1:1 wt ratio) were prepared by light milling. In the case of LSGM provided by Northwestern University (Scott Barnett), however, because the samples were supplied as sintered discs, the diffraction experiments were performed directly on one of these discs, after having deposited porous BSCF onto it via colloidal spray deposition. The BSCF deposition methods are described below. Diffraction data were collected at 825 and 950 °C after a dwell time of 5 or 6 hrs, conditions corresponding to those for processing symmetric samples, as also described below.

The results, Figures 2 to 4, indicate some surprising differences between the reactivity of different LSGM powders with BSCF. The Ceramatec LSGM shows strong evidence of reaction with BSCF, particularly at 950 °C. In both the 825 and 950 °C data the patterns contain a signficant impurity peak at 29° 2Θ, from a phase which remains to be identified. Furthermore, the overall shape of the peaks for the sample held at 950 °C are rather broad, suggesting intermediate phases with intermediate cubic lattice constant between LSGM (a = 3.917(4) Å) and BSCF (a = 3.9865(1) Å). In contrast, for the Caltech prepared LSGM no evidence for interdiffusion or reaction appears at 825 °C. At 950 °C, however, well-defined peaks between those of LSGM and BSCF appear, again suggesting the occurrence of a new perovskite phase with intermediate composition between LSGM and BSCF. Turning to the LSGM provided by Northwestern, in this case there are no additional peaks at either 950 or 825 °C. Furthermore, the peaks remain sharp and well-separated. While this may reflect the fact that in this case the powders were not directly mixed, it is quite probably that differences in processing render the Northwestern LSGM more robust against reaction with BSCF.

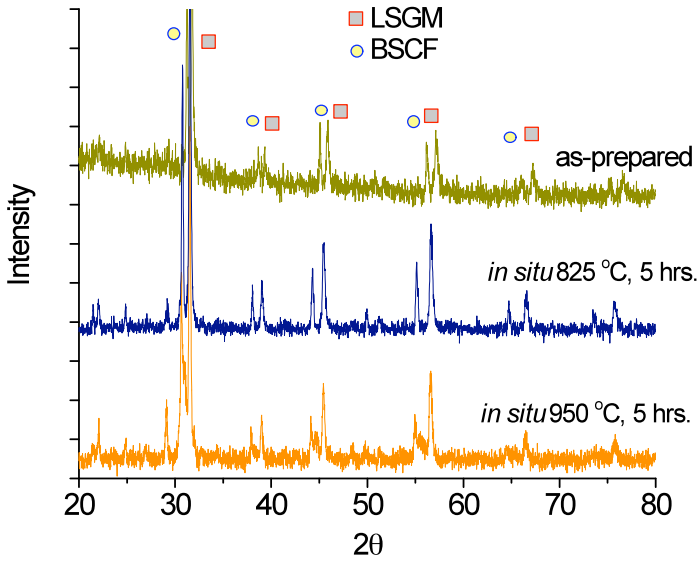

Figure 2. X-ray diffraction patterns obtained from mixtures of Ceramatec-LSGM and BSCF.

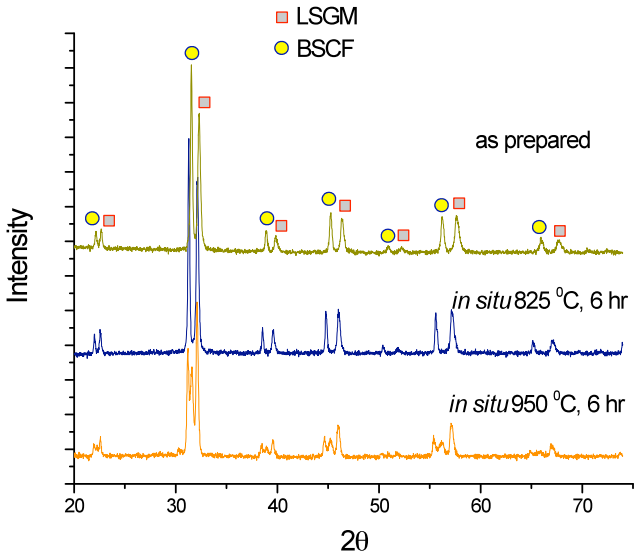

Figure 2. X-ray diffraction patterns obtained from mixtures of Caltech-LSGM and BSCF.

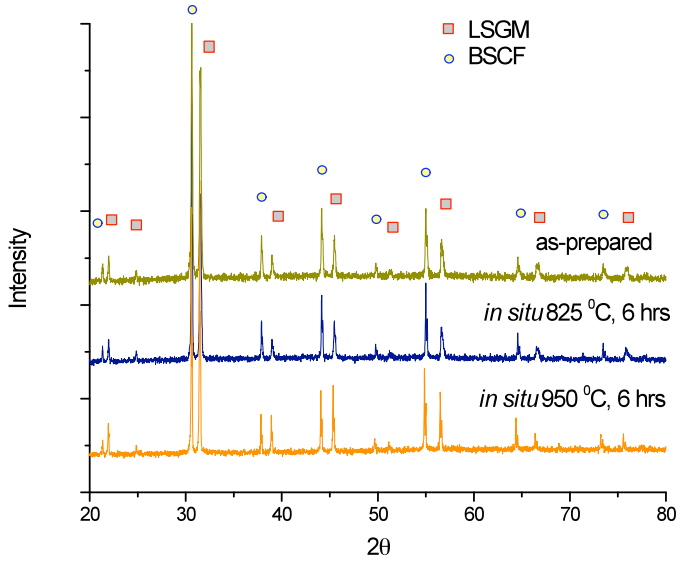

Figure 4. X-ray diffraction patterns obtained from NWU-LSGM in pellet form, onto which BSCF powder was applied.

Electrochemical Characterization

Procedures

Electrochemical characterization was performed on symmetric cells in which porous BSCF-based electrodes were applied to both sides of a dense electrolyte disc, with the latter prepared as follows. Approximately 1 g of the LSGM powder was pressed uniaxially in a 15-mm die under a weight of 5 tons (450 MPa). Sintering was carried out at 1550°C under stagnant air for 5 hours yielding discs with 96% density (Ceramatec powder) and 98% density (CIT-LSGM powder) and final diameter and thickness of 13 and 1 mm, respectively. In order to improve the subsequent adhesion of the cathode electrodes, in some instances (as specified below) a porous layer of the electrolyte material itself was first applied to both sides of the densified electrolyte disc. For this purpuse, the LSGM powder was suspended in a mixture of isopropanol, ethylene glycol, and glycerin and a thin layer of electrolyte powder was sprayed onto each face of the pellet. Spraying of one face of the pellet was followed by heat-treatment at 950°C for 5 hours, before proceeding to apply the electrolyte porous layer to the second side, which was then also heat treated at 950 °C for 5 hours. The porous layers so prepared are approximately 25 μm in thickness.

Subsequent to electrolyte deposition, the BSCF cathode powder was deposited using, again, a colloidal suspension in a mixture of isopropanol, ethylene glycol, and glycerin (ratios). Prior to deposition, the outer rim of each face of the cell was masked, leaving an exposed circular area of 0.71 cm^2 for cathode deposition. Volumes of the BSCF suspension ranging from 2 μl to 8 μl were applied to one face of each cell at a time, followed by heat treatment at either 950°C or 825 °C for 5 hours before proceeding to apply the cathode to the opposite side (using an equal volume of cathode slurry and an additional heat treatment step). In general, it was observed that for heat treatment at 825 °C, prior application of the porous electrolyte layer was required in order to obtain sufficient adhesion between the electrolyte and cathode layers. To facilitate current exchange across the entire cathode surface, a dilute slurry of silver paste (Ted Pella, 16032), mixed with SiO_2 powder to prevent sintering of the colloidal silver under high

temperature, was spread over the surface of each face of the cathode. A small section of silver mesh gauze (Alfa Aesar, 40936) affixed to silver wire (Alfa Aesar, 12187) served as the electrode lead and was attached to the cathode material using the same viscous silver paste.
In addition to the evaluation of BSCF on LSGM, selected measurements were performed using the cathode $La_{0.6}Sr_{0.4}Co_{0.2}Fe_{0.8}O_{3-\delta}$ (LSCF). In this case, a LSCF + LSGM composite paste, consisting of LSGM and LSCF powders in a weight ratio of 7:3 in a Heraeus vehicle (V-737), was supplied by Northwestern University. The viscous paste was directly applied onto LSGM pellets, also provided by Northwestern University, with an area of 0.71 cm^2 and fired at 950 °C. Finally, as in the case of the BSCF based cells, a porous silver conductive layer (Ag + SiO_2 slurry) was painted over the cathode, and silver mesh and wire were attached as current collectors.
Two-probe AC EIS was executed on either a Solartron 1260 or Solartron 1250 impedance analyzer with an amplitude of 10 mV. The frequency was allowed to range from 0.01 Hz to 60 kHz on the Solartron 1250, and between 0.01 Hz and 1 MHz on the Solartron 1260. Inductance created by the silver paste current collectors and silver wire leads were measured separately and subtracted. Impedances were measured from 475 °C to 725 °C in increments of 25 °C. Gas flows were regulated by mass flow controllers at a total flow rate of 100 sccm. Oxygen partial pressure was kept at 0.21 atm in an O_2/N_2 mixed atmosphere. Typical impedance spectra as plotted in the Nyquist representation, Zr(w) vs. -Zi(w), displayed two arcs (examples are shown below). The first, an incomplete arc which was readily extrapolated to the origin, was assigned to the electrolyte behavior and the second, a complete arc occuring at lower frequencies, was assigned to the electrochemical behavior of the cathode. From the diameter of this lower frequency arc the cathode area specific polarization resistance (R_P) was determined.

Results

A comparison of the cathode R_P for several cells is presented in Figure 5, emphasizing the impact of processing temperature and the difference in behavior of BSCF on different electrolyte materials. Data are shown specifically for (a) BSCF-950 on Ceramatek LSGM; (b) BSCF-825 on Ceramatek LSGM; (c) BSCF-950 on Caltech LSGM; (e) BSCF-825 on Caltech LSGM; (e) BSLCFG-950 on SDC; and (f) BSCF-950 on SDC, where the number indicates the heat treatment temperature. All samples were prepared using 6 μl of colloidal suspension and a porous electrolyte interlayer to facilitate adhesion. It is immediately apparent that a heat treatment temperature of 950 °C on the Ceramatek LSGM dramatically increases the cathode polarization resistance relative to that at 825. This increase is about one order of magnitude. In contrast, heat treatment temperature has little influence on the polarization resistance of BSCF on Caltech-prepared LSGM, and the resistance of these sample lie intermediate between the two Ceramatek-based samples. The similarity of the two Caltech-based samples suggests that there should not be major microstructural differences induced by the difference in heat treatment temperatures (such as loss of surface area) that could explain the difference in the two Ceramatek-based samples. Direct introduction of La and Ga into BSCF, as reflected in the cathode composition BSLCFG, similarly has little impact on the polarization resistance and even this new composition has excellent activity on SDC. Thus, possible incorporation of foreign La and Ga atoms into BSCF at high processing temperatures is apparently not responsible for the difference either. These observations lead us to conclude that some other detrimental interaction between BSCF and the Ceramatek LSGM, as reflected in the high temperature x-ray diffraction data, Figure 2, is responsible for the poor catalytic activity after high temperature processing.

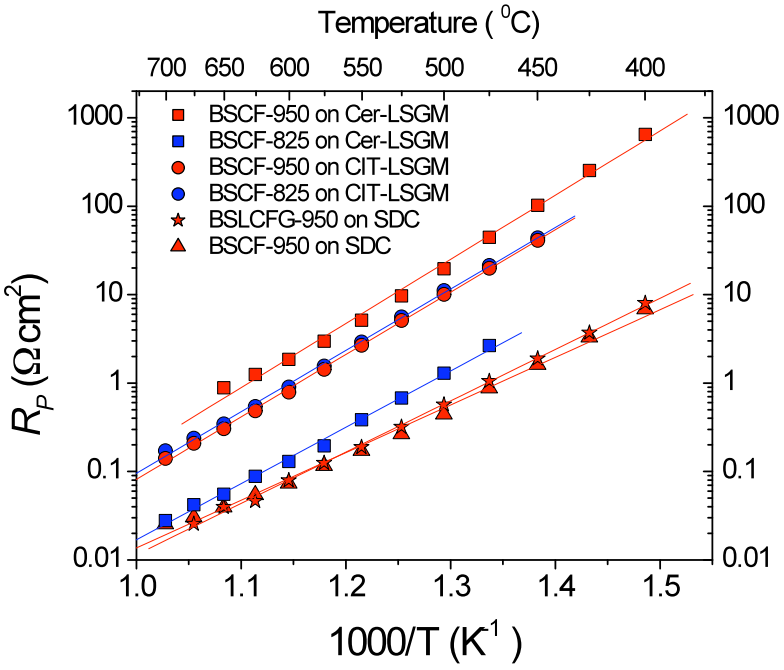

Figure 5. A comparison of the polarization resistances of several symmetric cells with cathode and electrolyte as indicated. Three digit numbers refer to cell fabrication temperature and BSLCFG is $Ba_{0.45}Sr_{0.45}La_{0.1}Co_{0.72}Fe_{0.18}Ga_{0.1}O_{3-\delta}$.

At this stage, the electrochemical behavior of BSCF on LSGM as it relates to processing conditions is not entirely understood. However, the similarity of the activation energy of the polarization resistance for the various different combination of LSGM sources and symmetric cell processing temperatures suggests that the mechanistic pathway is the same in all the systems and that differences in the absolute values of R_P are related to differences in the density of active sites. In the case of BSCF on SDC, we have shown elsewhere that surface exchange (at the interface between the BSCF and the gas phase) is the rate-limiting step in the oxygen electroreduction reaction, with oxygen transport through the BSCF itself being extremely rapid. The significance of incorporating a porous interlayer between the dense electrolyte and the cathode material is shown in Figure 6. Because of the impossibility of obtaining good adhesion in the absence of a porous interlayer for calcination at 825 °C, the comparisons are provided for calcination at 950 °C only, for both Ceramatek and Caltech LSGM. In all cases, 6 µl of cathode solution was utilized. It is apparent that the porous interlayer decreases the polarization resistance by a factor of 3-8 for both cases. We attribute this to the improved adhesion that occurs in the presence of this interlayer. It is noteworthy that in other experiments in which the entire cathode is replaced by a composite of BSCF and the electrolyte, the polarization resistance decreases and thus there is some limit to the benefits that are to be gained via the presense of an interlayer that ultimately contains both the electrolyte and BSCF.

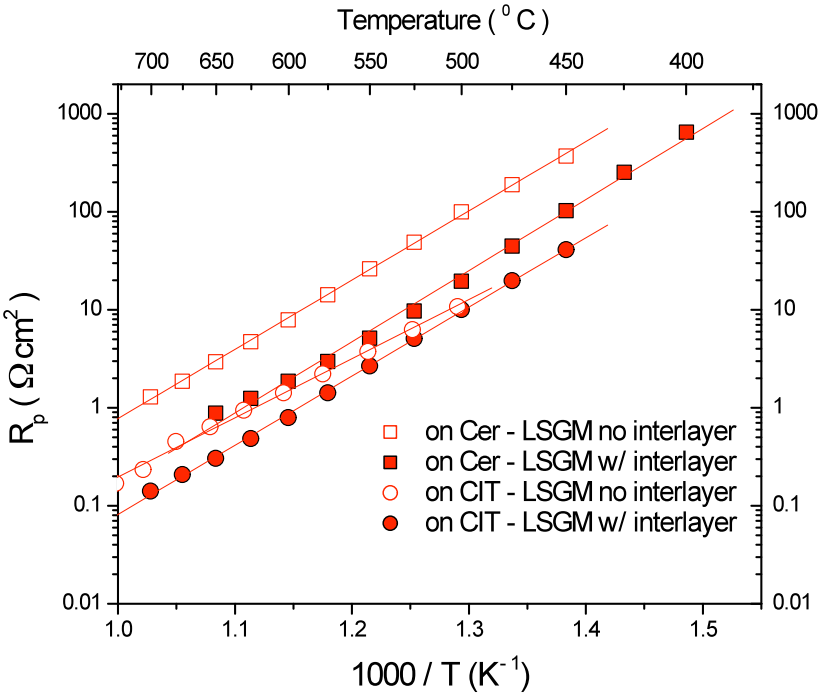

Figure 6. Polarization resistance of otherwise identical symmetric cells prepared with and without a porous interlayer of electrolyte between the dense electrolyte and porous BSCF cathode.

The selection of 6 μl of cathode solution has been predicated on the observation that increasing the cathode amount within the range of 2 – 6 μl generally decreases the polarization resistance, with limited benefit at larger amounts. This behavior is evident in Figure 7, which shows the reduction of R_P with increasing cathode amount for BSCF deposited onto both Ceramatek and Caltech LSGM. Fabrication of the Ceramatek based cells was performed using a porous interlayer and a heat treatment temperature of 825 °C. In contrast, the Caltech based cells were prepared without an interlayer and heat treated at 950 °C. While overall the polarization resistance is lower for the LSGM based cell, presumably as a result of the slightly different processing conditions, both sets show the cathode polarization resistance to decrease with increasing cathode thickness. This result is consistent with surface exchange at the cathode|gas interface being the rate-limiting step.

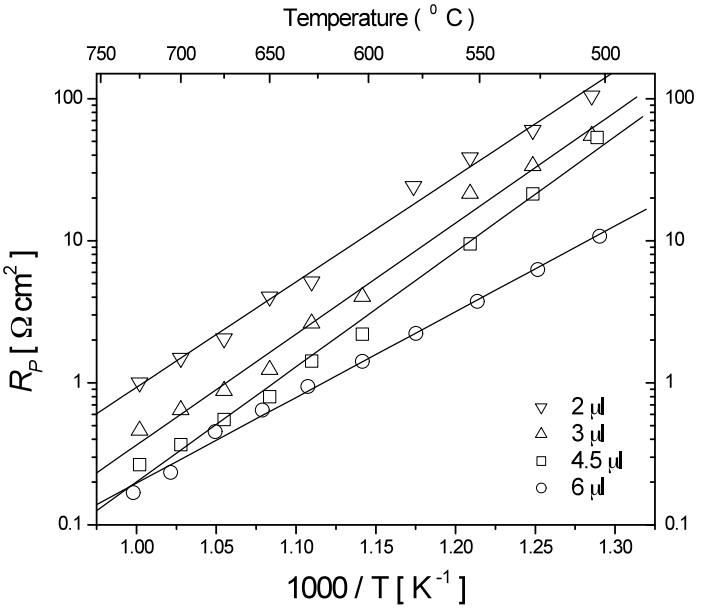

(a)

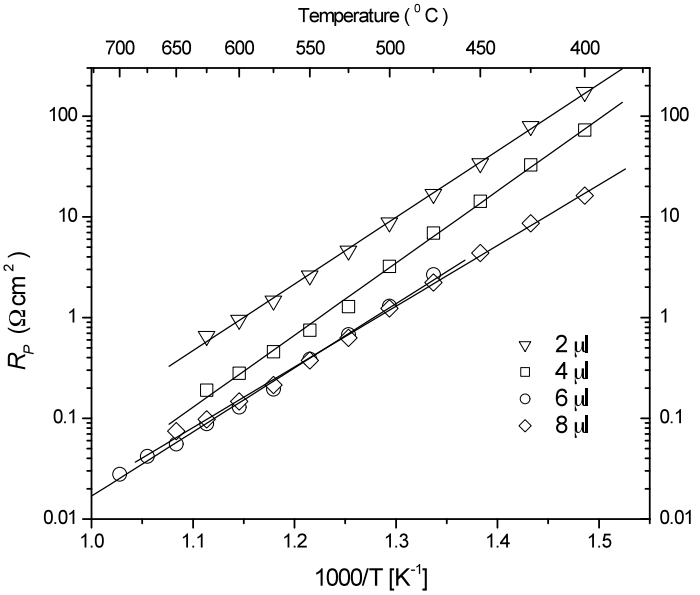

(b)

Figure 7. Reduction of R_P with increasing cathode amount for BSCF deposited onto (a) Ceramatek and (b) Caltech LSGM. The Ceramatek-LSGM cells included a porous interlayer and were processed at 825 °C. The Caltech-LSGM cells were prepared without an interlayer and were processed at 950 °C.

While the performance of BSCF on LSGM has not yet been tuned to match its performance on SDC, as discussed above with respect to Figure 5, it is noteworthy that BSCF does apparently provide higher electrochemical activity on LSGM than does LSCF. As shown in Figure 8, the LSCF + LSGM powder on NWU-LSGM displays a slightly greater polarization resistance than the BSCF powder on CIT-LSGM (processed at 950 °C) and a substantially greater polarization resistance than the BSCF powder on Cer-LSGM (processed at 825 °C).

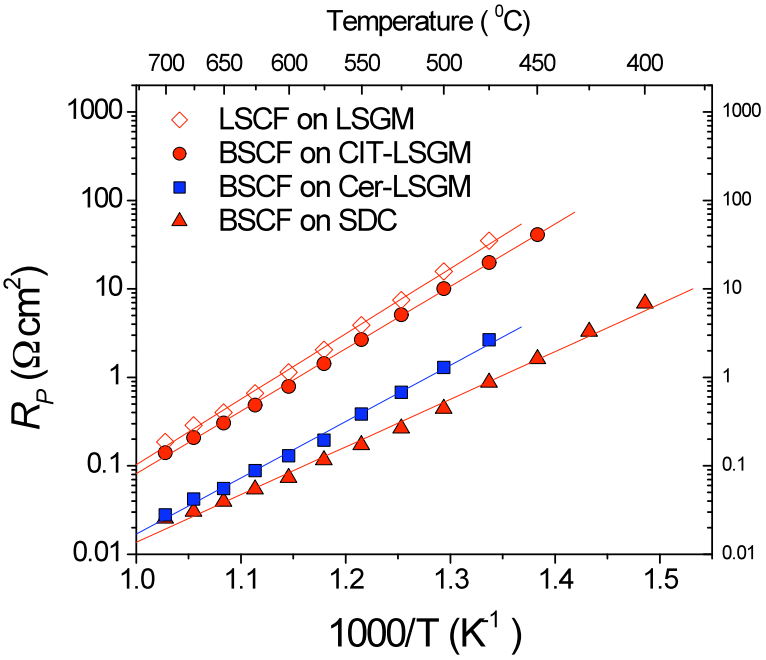

Figure 8. Comparison of the polarization resistance of various cells, where the highest performance cells of each type have been selected.

Conclusions

The new cathode material BSCF performs well on LSGM powder. Some issues with reactivity between the two remain to be addressed. With optimization of the fabrication procedures, exceptionally high power density fuel cells can be expected.